Statistical Analysis of Steady State Response in RF Circuits via Decoupled Generalized Polynomial Chaos

by

Seyed Ghavamoddin Nabavi

Thesis submitted to the
Faculty of Graduate and Postdoctoral Studies
In partial fulfillment of the requirements
For the M.A.Sc degree in
Electrical and Computer Engineering

School of Electrical Engineering and Computer Science
Faculty of Engineering
University of Ottawa

Abstract

One of the major factors in RF circuit design is the ability to predict the performance of these circuits in the presence of uncertainty in the key design parameters. This is referred to as uncertainty quantification in the mathematical literature. Uncertainty about the key design parameters arises mainly from the difficulty of controlling the physical or geometrical features of the underlying design, especially at the nanometer level. With the constant trend to scale down the process feature size, uncertainty quantification becomes crucial in shortening the design time.

This thesis presents a new approach to statistically characterize the variability of the Harmonic Balance analysis and its application to Intermodulation distortion analysis in the presence of uncertainty in the design parameters. The new approach is based on the concept of Polynomial Chaos (PC) and Stochastic Galerkin (SG) methods. However, unlike the traditional PC, the proposed approach adopts a new mathematical formulation that decouples the Polynomial Chaos problem into several problems whose sizes are equal to the size of the original Harmonic Balance problem. The proposed algorithm produces significant CPU savings with equivalent accuracy to traditional Monte Carlo and standard PC approaches.

Acknowledgments

I would like to express my sincerely gratitude to my supervisor, Professor Emad Gad for his great support and encouragement in my research. I am truly grateful for his valuable advices and inspirations, which were the keys to me finishing my research. I also appreciate Prof. Michel Nakhla and Prof. Ram Achar my Co-supervisors for their huge support during my education.

I wish to thank my colleague Chen who was a great help in this thesis. I want to give my special thanks to my wife and my daughter, Narges and Khorshid, for their understanding, respect, companionship and huge support they provided me during my education. It is because of them that I could overcome difficulties during my work. I also wish to thank my family, specially my mother who always is there for me when I need her.

Table of Contents

List of Tables

List of Figures

List of Acronyms

Acronyms	Definition
CAD	Computer Aided Design
CPU	Central Processing Unit
EM	Electromagnetic
GP	Galerkin Projection
gPC	Generalized Polynomial Chaos
HB	Harmonic Balance
HB-PC	Polynomial Chaos Applied to Harmonic Balance analysis
IIP3	3rd order input intercept point
IIP2	2nd order input intercept point
IMD	Intermodulation Distortion
MNA	Modified Nodal Analysis
MC	Monte Carlo Analysis
PC	Polynomial Chaos
pdf	Probability Density Function
PDF	Probability Distribution Function
RF	Radio Frequency
SC	Stochastic Collocation Method

List of Symbols

Symbols	Definition
$\boldsymbol{b}$	Vector representing input excitation in time domain
$\bar{\boldsymbol{B}}$	A vector containing Harmonics of input excitations
$\boldsymbol{C}$	matrix describing the memory elements in the circuit
$\boldsymbol{E}$	Expected Value
$\boldsymbol{f}(\boldsymbol{x}(t))$	Vector including nonlinear components of circuit in time domain
$\bar{\boldsymbol{F}}(\bar{\boldsymbol{X}})$	Nonlinear vector in HB equation
$\boldsymbol{G}$	matrix describing the memoryless elements in the circuit
H	Number of Harmonic Coefficients
H_i	i^{th} volterra kernell
$\boldsymbol{\mathcal{H}_\alpha}$	Hermite polynomials
$\bar{\boldsymbol{J}}$	Jacobian matrix in HB analysis
$\boldsymbol{\mathcal{J}}_{HB}$	Total jacobian matrix in HB analysis
$\bar{\boldsymbol{J}}_0$	Jacobian matrix in the absences of RF stimulus
$\bar{\boldsymbol{J}}_k$	k^{th} Taylor moment of Jacobian matrix $\bar{\boldsymbol{J}}$
$\boldsymbol{\mathcal{J}}_{HB-PC}$	Total jacobian matrix in HB-PC approach
$\tilde{\boldsymbol{\mathcal{J}}}_{HB-PC}$	Total jacobian matrix in decoupled HB-PC approach
K	Number of Harmonics
$\boldsymbol{\mathcal{M}}$	Taylor coefficients of HB response
N	Number of circuit variables

Symbols	Definition
var	Variance
$w(\xi)$	Weighting function for single-dimensional polynomial
$\boldsymbol{w}(\boldsymbol{\xi})$	Weighting function for multi-dimensional polynomial
$\bar{\boldsymbol{X}}$	Vector containing Harmonics for circuit variables
$\boldsymbol{x}(t)$	Circuit response in time domain
$\boldsymbol{\mathcal{X}}$	gPC coefficients of Harmonic Balance response
$\boldsymbol{Y}$	Matrix containing linear component in HB analysis
$\boldsymbol{\mathcal{Y}}$	gPC coefficients of matrix $\boldsymbol{Y}$
$\boldsymbol{\alpha}$, $\boldsymbol{\beta}$, $\boldsymbol{\gamma}$	Multi-dimensional indices
α, β, γ	Single-dimensional indices
α_i	i^{th} component of $\boldsymbol{\alpha}$
$\delta_{\boldsymbol{\alpha},\boldsymbol{\beta}}$	Kronecker delta function
ξ	Single random variable
$\boldsymbol{\xi}$	set of multi random variable
$\phi_\alpha(\xi)$	Single-dimensional polynomial with degree α
$\phi_{\boldsymbol{\alpha}}(\boldsymbol{\xi})$	Multi-dimensional polynomial with degree $\boldsymbol{\alpha}$
$\otimes$	Kronecker product operator
Γ	Discrete Fourier Transform matrix
ω	Angular frequency
$\boldsymbol{\chi}$	Support
$<,>$	Inner Product

Chapter 1

Introduction

1.1 Background

One of the main challenges facing the designer of radio frequency integrated circuits is predicting the effect of the variability of geometrical and physical parameters on the circuit performance. Although the Monte Carlo (MC) simulations have been traditionally used in commercial circuit and Electromagnetic (EM) simulations to predict the statistical distribution of circuit and system performance metrics (e.g. gain, intermodulation distortion), their slow convergence has become a computational burden, especially when the simulation task is to perform steady-state analysis of a large circuit with multi-tone excitation using the notion of Harmonic Balance (HB) [1, 2, 3, 4, 5, 6, 7, 8, 9, 10, 11]. This fact has prompted wide interest in exploring alternative approaches to the problem of statistical analysis of the performance of electronic circuits in general.

A recent approach based on the concept of Polynomial Chaos (PC) [12] was developed and showed great computational advantage over the standard MC-based analysis [13]. The basic idea

in this approach is to expand the system variables as a series of Wiener-Askey-type orthogonal polynomials in the uncertain design parameters, and solve for the coefficients of the expansion. Those coefficients are then used to compute the statistical properties of the performance metrics. Although, the resulting mathematical problem of the PC approach is larger than the original analysis problem (e.g. the HB problem in this context), the fact that it needs to be solved only once brings a significant computational advantage when compared with the MC-based simulations.

Unfortunately, the computational advantage of the PC approach is quickly lost when the circuit has a large number of uncertain design parameters. This problem is even more amplified when the goal is to use the PC approach to statistically characterize the results of the HB problem (henceforth referred to as HB-PC). The difficulty in HB-PC mainly stems from the fact that the HB problem is larger in size and denser in structure than typical circuit simulation problems, especially in the presence of strong nonlinear behaviour, and several non-commensurate tones in the circuit stimulus.

This fact makes the size of the Jacobian matrix of the nonlinear HB-PC problem grows quickly beyond the typical memory resources even for very small number of uncertain design parameters. The goal of this thesis is to address the above discussed computational disadvantage in the HB-PC.

Intermodulation Distortion (IMD) is an essential concern in the course of RF circuit design, that is a pivotal metric of linearity for a wide range of nonlinear RF Circuits and its characterization is often considered as the main objective in design. The traditional approaches often employed to analyze IMD are either based on complex Volterra Kernels analysis or built upon a Harmonic Balance simulation with a naturally dense Jacobian matrix.

When design uncertainties need to be considered in computing IMD, it needs to be analysed statistically to characterize its variability from the nominal design.

In this situation, MC approach has been traditionally applied to above mentioned IMD analysis methods and used to quantify variability in circuit performance when design uncertainties are taken into account. However, as mentioned above its quantification process usually converges after performing tones of simulations. Consequently, stochastic methods based on the generalized Polynomial Chaos act as a suitable alternative [13].

1.2 Motivation

The fact that the traditional methods based on MC and PC approaches could be very slow in performing uncertainty quantification of RF circuits, especially, when analyzing circuits having more than one stimulus such as mixers, is the main motivation of this work. Moreover, seeking a fast method in order to statistically analyze the intermodulation distortion, IIP3, IIP2, etc, of RF circuits is additional motivation of this work.

1.3 Contribution

The main feature of the first contribution of the work presented in this thesis is that it enables the PC approach to handle large number of design variables without incurring the growth in the computational cost with the increase in the number of design parameters. The main idea in the proposed approach can be described as a two-step process. In the first step, a closed-form description for the Jacobian matrix of the nonlinear HB-PC problem is derived. The closed-form

analytical formula derived for this matrix reveals important structural properties that are used, in the second step, to develop an alternative Jacobian matrix whose structure is block diagonal. The factorization of the alternative matrix is much faster than the original Jacobian, since it can be decoupled into the factorizations of the diagonal blocks [14]. It should also be noted that the basic theory of decoupling the problem of polynomial chaos was introduced by the authors in [15] where it was used in the variability analysis of high-speed interconnect and packaging systems.

The second contribution of the work presented in this thesis is to address difficulties in analysing IMD in RF circuits in the presence of uncertainties. This contribution is based on applying the above two-step approach to a recently developed [16] Moment-based technique to compute the Volterra kernels. The special case of a single random design parameter was presented in [17] while this thesis provides the generalization to multi-dimensional random spaces along with the required proofs.

1.4 Organization of the Thesis

The rest of the thesis is organized as follow, a background on Harmonic Balance (HB) and its applications in analysing Intermodulation Distortion (IMD) is presented in next chapter. The Chapter 3 illustrates preliminary concepts of statical analysis in RF circuits, moreover, some standard methods in characterizing the behavior of such circuits with the presence of design uncertainties along with their limitations will be summarized. Chapter 4 presents the core of the proposed decoupling method aimed to overcoming the limitations of standard statistical analysis method in HB approach along with required proofs. Chapter 5 exhibits the application of the

proposed method in statistically analyzing the Intermodulation Distortion of RF circuits. Finally, chapter 6 presents the numerical results validating both proposed ideas.

Chapter 2

Background of Harmonic Balance Approach and its Applications in Analysing IMD

Section 2.1 presents the mathematical formulation for general nonlinear circuits followed by the basic concepts of Harmonic Balance approach used in steady state analysis of RF circuits. This will be followed by a brief review of traditional methods of Intermodulation distortion analysis and a recently efficient method based on a moment based Harmonic Balance approach .

2.1 Mathematical formulation of HB approach

The rapid growth in RF silicon integrated circuits (ICs) for mobile communication systems has placed new demands on the simulation tools. Quantities such as intermodulation and harmonic

distortion are typically of interest to circuit designers. However, finding the steady-state response for large analog and RF nonlinear circuits has always been a challenge. The reason for this is that these circuits usually exhibit characteristics that make most traditional transient based time-domain approaches perform poorly. For instance, if there are widely separated time constants in the circuit, then the usual transient analysis can take many clock cycles before the steady-state solution is reached.

The harmonic-balance (HB) technique [18, 19, 20, 21], has been introduced to address the above difficulties. The main concept behind HB is that waveforms in a periodically excited nonlinear circuit are periodic and, therefore, can be represented in the frequency domain as a finite Fourier series. In effect, this transforms the differential equations describing the circuit into a set of nonlinear algebraic equations that can be solved directly using iterative techniques such as the Newton Raphson (NR) method. Mathematical formulation of nonlinear circuits in time-domain formulation is given by using Modified Nodal Analysis (MNA) as,

$$\boldsymbol{C}\frac{d\boldsymbol{x}(t)}{dt} + \boldsymbol{G}\boldsymbol{x}(t) + \boldsymbol{f}(\boldsymbol{x}(t)) = \boldsymbol{b}(t) \tag{2.1}$$

where $\boldsymbol{G}$ and $\boldsymbol{C} \in \mathbb{R}^{N\times N}$ are matrices describing the memoryless and memory elements in the circuit, respectively, $\boldsymbol{x}(t) \in \mathbb{R}^N$ is a vector of circuit response (e.g., nodes voltages and inductors currents), and $\boldsymbol{b}(t) \in \mathbb{R}^N$ in the above formulation represents the time-domain vector of independent sources. $\boldsymbol{f}(\boldsymbol{x}(t))$ is the vector of nonlinear algebraic function that captures the nonlinear elements in the circuit.

Consider the MNA formulation (2.1), HB approach assumes that all source excitation in $\boldsymbol{b}(t)$ are periodic having a period $\boldsymbol{T}$ with a Fourier series expansion of $\boldsymbol{K}$ harmonics, consequently $\boldsymbol{f}(\boldsymbol{x}(t))$, $\boldsymbol{b}(t)$ and $\boldsymbol{x}(t)$ can be written in finite Fourier series as follow:

$$\boldsymbol{x}(t) \;=\; \boldsymbol{X}_0 + \sum_{m=1}^{K} \boldsymbol{X}_m^C cos(m\omega t) + \boldsymbol{X}_m^S sin(m\omega t) \tag{2.2}$$

$$\boldsymbol{f}(\boldsymbol{x}(t)) \;=\; \boldsymbol{F}_0 + \sum_{m=1}^{K} \boldsymbol{F}_m^C cos(m\omega t) + \boldsymbol{F}_m^S sin(m\omega t) \tag{2.3}$$

$$\boldsymbol{b}(t) \;=\; \boldsymbol{B}_0 + \sum_{m=1}^{K} \boldsymbol{B}_m^C cos(m\omega t) + \boldsymbol{B}_m^S sin(m\omega t) \tag{2.4}$$

where $\boldsymbol{X}_m^{C,S}$, $\boldsymbol{F}_m^{C,S}$ and $\boldsymbol{B}_m^{C,S}$ represent the m^{th} Fourier coefficients of $\boldsymbol{x}(t)$,$\boldsymbol{f}(\boldsymbol{x}(t))$ and $\boldsymbol{b}(t)$ respectively.

By sampling (2.2) at discrete time points, a concrete relation between the time domain and Frequency domain can be obtained as follows,

$$\boldsymbol{x}(t) = \Gamma^{-1}\boldsymbol{X}, \tag{2.5}$$

where, Γ^{-1} is an orthogonal matrix given by:

$$\Gamma^{-1} = \begin{bmatrix} 1 & cos(\omega t_0) & sin(\omega t_0) & ... & sin(K\omega t_0) & cos(K\omega t_0) \\ 1 & cos(\omega t_1) & sin(\omega t_1) & ... & sin(K\omega t_1) & cos(K\omega t_1) \\ . & . & . & ... & . & . \\ . & . & . & ... & . & . \\ . & . & . & ... & . & . \\ 1 & cos(\omega t_{2K}) & cos(\omega t_{2K}) & ... & cos(K\omega t_{2K}) & cos(K\omega t_{2K}) \end{bmatrix}$$

Here, Inverse Discrete Fourier Transform (IDFT) matrix Γ^{-1} converts 2K+1 fourier domain coefficients to its time domain representation. HB approach then proceeds by using above formulations in order to construct the frequency domain MNA equations as follows,

$$\boldsymbol{Y}\bar{\boldsymbol{X}} + \bar{\boldsymbol{F}}(\bar{\boldsymbol{X}}) = \bar{\boldsymbol{B}}, \tag{2.6}$$

where $\bar{\boldsymbol{X}} \in \mathbb{R}^{NH}$ is a vector containing H (unknown) Harmonics for N circuit variables, $\boldsymbol{Y} \in \mathbb{R}^{NH \times NH}$ and $\bar{\boldsymbol{F}}(\boldsymbol{X}) \in \mathbb{R}^{NH}$ capture the linear and nonlinear parts in the circuit, respectively. Here $\bar{\boldsymbol{B}} \in \mathbb{R}^{NH}$ represents all the independent sources in the circuit and $H = 2K+1$. Solving the system (2.6) can be carried out using either continuation method or Newton Raphson iterations.

2.1.1 Newton Raphson Method (NR)

In the NR method the solution of (2.6) is iteratively updated in the following manner, starting with an appropriate initial guess $\bar{\boldsymbol{X}}^{(0)}$,

$$\bar{\boldsymbol{X}}^{n+1} = \bar{\boldsymbol{X}}^{n} + \boldsymbol{\mathcal{J}}_{HB}^{-1}\boldsymbol{\phi}, \tag{2.7}$$

where,

$$\boldsymbol{\phi} = \boldsymbol{Y}\bar{\boldsymbol{X}} + \bar{\boldsymbol{F}}(\bar{\boldsymbol{X}}) - \bar{\boldsymbol{B}}, \tag{2.8}$$

Here, $\boldsymbol{\mathcal{J}}_{HB}$ is the total jacobian matrix constructed as follows:

$$\boldsymbol{\mathcal{J}}_{HB} = \frac{\partial \boldsymbol{\phi}}{\partial \bar{\boldsymbol{X}}} = \boldsymbol{Y} + \bar{\boldsymbol{J}} \tag{2.9}$$

where, it can be shown, based on the derivations in [19], that the matrix $\bar{\boldsymbol{J}} = \frac{\partial \bar{\boldsymbol{F}}(\bar{\boldsymbol{X}})}{\partial \bar{\boldsymbol{X}}} \in \mathbb{R}^{NH \times NH}$ of the nonlinear term (2.6) can be described as follows,

$$\bar{\boldsymbol{J}} = \bar{\boldsymbol{\Gamma}} \left(\sum_{m=1}^{K} \boldsymbol{J}\left(\boldsymbol{x}_m\right) \otimes \overbrace{\mathbf{e}_{m,K}\mathbf{e}_{m,K}^{\top}}^{\in \mathbb{R}^{K \times K}} \right) \bar{\boldsymbol{\Gamma}}^{-1} \tag{2.10}$$

Here, $\otimes$ denotes the kronecker product, and $\mathbf{e}_{m,K}$ represents the m^{th} column in a $K \times K$ identity matrix.

The major time-consuming part is spent in factorizing the Jacobian matrix $\boldsymbol{\mathcal{J}}_{HB}$ due to its large size and dense structure. Also, NR method could encounter difficulties in convergence if the initial guess used to solve (2.7) has not been chosen appropriately.

2.1.2 Continuation Method

Continuation methods are used to overcome the convergence problems associated with the iterative techniques such as the NR method described above. The basic idea in using the continuation methods in the contest of HB starts by recasting (2.6) as follows:

$$\boldsymbol{Y}\bar{\boldsymbol{X}} + \bar{\boldsymbol{F}}(\bar{\boldsymbol{X}}) = \bar{\boldsymbol{B}}_{dc} + \alpha\bar{\boldsymbol{B}}_{RF}, \tag{2.11}$$

Here, $\bar{\boldsymbol{B}}_{RF}$ and $\bar{\boldsymbol{B}}_{dc}$ represent RF excitations and DC source respectively. The basic concept of continuation methods is that the parameter α will increase from 0 to 1 in small increments, where at $\alpha = 0$ the solution of(2.11) is simply DC solution while $\alpha = 1$ represents the same solution as (2.6). As can be clearly seen the continuation method does not suffer from the convergence problem, however, it suffers a significantly higher computational cost.

2.2 Intermodulation Distortion (IMD) analysis

One of the fundamental tasks often required in the course of designing of RF circuits is to analyse the Intermodulation Distortion such as 3rd order input intercept point (IIP3), 2nd order input

intercept point (IIP2). The main challenges in computing IIP3 analytically is the complexity of traditional approaches based on the Volterra Kernels [22] or computation cost of HB based Brute Force approach. In this section traditional methods in analyzing IMD are summarized and followed by a recently efficient Moment Based HB approach that can be used in order to calculate IIP3, IIP2 and Gain Compression, etc.

2.2.1 Standard methods of (IMD) analysis

Computing the Intermodulation Distortion (IMD) caused by nonlinearity in the system is typically carried out by considering an RF stimulus of the form $\boldsymbol{V}_{RF} = \boldsymbol{A}\cos(\omega_1 t) + \boldsymbol{A}\cos(\omega_2 t)$. IMD can then be characterized analytically using the Volterra series expansion, where, in this method, circuit response is expanded in Volterra series as follows,

$$\boldsymbol{y(t)} = \sum_{i=0}^{\infty} H_i(\boldsymbol{V}_{RF}(t)) \tag{2.12}$$

where H_i is the i^{th}-order Volterra operator [22]. Once the Volterra operators are derived, IMD properties such as 1-dB gain compression $\text{P}_{1-\text{dB}}$, $3rd$ order input intercept point IIP3 or $2nd$ order input intercept point IIP2 [22], can be calculated using following expressions,

$$\text{IIP3} = \sqrt{\frac{4|H_1(j\omega_1)|}{3|H_3(j\omega_1, j\omega_1, -j\omega_2)|}} \tag{2.13}$$

$$\text{IIP2} = \frac{|H_1(j\omega_1)|}{|H_2(j\omega_1, -j\omega_2)|} \tag{2.14}$$

$$\text{P}_{1-\text{dB}} \approx \text{IIP3} - 9.6\text{dB}. \tag{2.15}$$

Typically, deriving analytical expressions for the Volterra kernels is very cumbersome in general circuits. In order to avoid such analytical derivations, circuit designers and Computer-

Aided Design (CAD) tools resort to the numerical computation of the IMD products using the HB approach. This idea is explained next.

In the HB-based IMD analysis, circuit is represented in the frequency-domain using the HB equations (2.6). Computing IMD properties, such as IIP3, in this method is carried out by first solving the above HB equations using an iterative Newton method for a given input power P_{in}. Next, the output powers at the fundamental frequency and at the third-order intermodulation respectively, denoted by $P_{\text{out}}(\omega_1)$ and $P_{\text{out}}(2\omega_2 - \omega_1)$, are extracted from this solution. Finally, this process is repeated for various values of P_{in}, and the intercept point between $P_{\text{out}}(\omega_1)$ and $P_{\text{out}}(2\omega_2 - \omega_1)$ is extrapolated to estimate IIP3.

The main computational cost in this method arises from having to factorize the Jacobian matrix, which has a typically large size and dense structure, repeatedly at different levels of input power. A recent approach has been presented in [16] to avoid the factorization of the HB Jacobian matrix. This approach is briefly described next.

2.2.2 Moment-based IMD analysis

This approach to computing the IMD starts by first splitting the stimulus part on the right side of (2.6) in two parts that correspond to the DC and RF stimulus as shown by

$$\boldsymbol{Y}\bar{\boldsymbol{X}}(\alpha) + \bar{\boldsymbol{F}}(\bar{\boldsymbol{X}}(\alpha)) = \bar{\boldsymbol{B}}_{\text{DC}} + \alpha\bar{\boldsymbol{B}}_{\text{RF}}, \tag{2.16}$$

Here, $\bar{\boldsymbol{B}}_{\text{DC}}$ is a vector representing the DC stimuli in the circuit. In the above equation, α is the amplitude of input signals and $\bar{\boldsymbol{B}}_{\text{RF}} \in \mathbb{R}^{NH}$ is a vector whose entries being 0 in the absence of the RF sources from the circuit and 1 in the presence of RF source. This method then proceeds

by expanding the HB response $\bar{\boldsymbol{X}}$ and nonlinear part $\bar{\boldsymbol{F}}(\bar{\boldsymbol{X}})$ as a Taylor Series in α, as shown next,

$$\bar{\boldsymbol{X}}(\alpha) = \sum_{n=0}^{q} \boldsymbol{\mathcal{M}}_n \alpha^n, \tag{2.17}$$

$$\bar{\boldsymbol{F}}(\bar{\boldsymbol{X}}(\alpha)) = \sum_{n=0}^{q} \hat{\boldsymbol{F}}_n \alpha^n, \tag{2.18}$$

where $\boldsymbol{\mathcal{M}}_n$ and $\hat{\boldsymbol{F}}_n$ are the Taylor series coefficients (or the moments) of HB response and nonlinear function, respectively.

It has been shown in [16] that the numerical values of the Volterra kernel at the frequency of excitation can be extracted from the moments $\boldsymbol{\mathcal{M}}_n$. Table 2.1 shows the mapping between the Volterra kernels and the moments of a circuit excited by two tones ω_1 and ω_2. In this table, a zero entry at moment $\boldsymbol{\mathcal{M}}_n$ and a frequency component at the response indicates no relation between the n^{t} moment and that frequency component.

Computing those moments is typically performed in three steps. In the first step, $\boldsymbol{\mathcal{M}}_0$ is computed by substituting from (2.17) and (2.18) into (2.16) and setting α to zero. This process yields the nonlinear systems

$$\boldsymbol{Y}\boldsymbol{\mathcal{M}}_0 + \bar{\boldsymbol{F}}(\boldsymbol{\mathcal{M}}_0) = \bar{\boldsymbol{B}}_{\text{DC}}, \tag{2.19}$$

which can be solved via the NR and using the Jacobian matrix,

$$\bar{\boldsymbol{J}}_0 = \boldsymbol{Y} + \left.\frac{\partial \bar{\boldsymbol{F}}(\bar{\boldsymbol{X}})}{\partial \bar{\boldsymbol{X}}}\right|_{\alpha=0} \tag{2.20}$$

Next, $\boldsymbol{\mathcal{M}}_1$ is computed by substituting from (2.17) and (2.18) into, (2.16), differentiating once with respect to α and setting $\alpha = 0$ to obtain

$$\bar{\boldsymbol{J}}_0 \boldsymbol{\mathcal{M}}_1 = \bar{\boldsymbol{B}}_{\text{RF}}, \tag{2.21}$$

Higher-order moments $\boldsymbol{\mathcal{M}}_n$ are computed in a likewise manner, where the the differentiation with respect to α is carried out n times, thereby yielding the system

$$\bar{\boldsymbol{J}}_0 \boldsymbol{\mathcal{M}}_n = -\frac{1}{n} \sum_{k=1}^{n-1} (n-k) \boldsymbol{J}_k \boldsymbol{\mathcal{M}}_{n-k}, \tag{2.22}$$

where $\boldsymbol{J}_k$ is the k^{th} Taylor series coefficient of the matrix $\partial \bar{\boldsymbol{F}}(\bar{\boldsymbol{X}})/\partial \bar{\boldsymbol{X}}$. Therefore, the main CPU cost of computing the moments, and in turn the Volterra kernels, is the factorization of the Jacobian matrix $\bar{\boldsymbol{J}}_0$. In fact, this matrix, being computed when the RF sources are deactivated (i.e., $\alpha = 0$), is equivalent to the Jacobian matrix of the circuit computed at the DC operating point. This fact represents the main advantage of this approach since this matrix is block diagonal making it easier to factorize compared with the HB full Jacobian matrix, which is typically much denser.

Table 2.1: Locations of Volterra kernels in the HB moments vector

Frequency	$\mathcal{M}_0$	$\mathcal{M}_1$	$\mathcal{M}_2$	$\mathcal{M}_3$
DC	H_0	0	$\frac{1}{2}\lvert H_2(j\omega_1, -j\omega_1)\rvert + \frac{1}{2}\lvert H_2(j\omega_2, -j\omega_2)\rvert$	0
$\lvert 2\omega_1 \pm \omega_2\rvert$	0	0	0	$\frac{3}{4}\lvert H_3(j\omega_1, j\omega_1, -j\omega_2)\rvert$
ω_1	0	$\lvert H_1(j\omega_1)\rvert$	0	$\frac{3}{2}\lvert H_3(j\omega_1, j\omega_2 - j\omega_2)\rvert + \frac{3}{4}\lvert H_3(j\omega_1, j\omega_1, -j\omega_1)\rvert$
$\lvert \omega_1 - \omega_2\rvert$	0	0	$\lvert H_2(j\omega_1, -j\omega_2)\rvert$	0
$\lvert 2\omega_2 \pm \omega_1\rvert$	0	0	0	$\frac{3}{4}\lvert H_3(j\omega_1, -j\omega_2, j\omega_2)\rvert$
$2\omega_2$	0	0	$\frac{1}{2}\lvert H_2(j\omega_2, j\omega_2)\rvert$	0

2.3 Discussion

Harmonic Balance simulation as a powerful numerical technique in simulating nonlinear circuits and its applications in characterizing Intermodulation distortion was discussed in this chapter. However, all presented equations were deterministic without considering design uncertainties in HB equation. HB simulation in the presence of uncertain parameters has to consider uncertainties in constructing (2.6). The next chapter presents a brief background on the subject of statistical analysis of RF circuits illustrating the main concepts that are related to this thesis.

Chapter 3

Statistical Analysis of RF Circuits

The previous chapter presented deterministic equations governing steady state analysis of RF circuits and its applications to characterize IMD. However, there exist many situations in which some parameters of RF circuit are unknown or hard to control and, therefore, have to be represented in terms of random variables with appropriate distributions. For instance, considering an RF circuit, there could be a difference between its nominal output at design level and its actual output after fabrication process due to uncertain parameters. As a result, the steady state response becomes a stochastic process itself and needs to be characterized statistically. Such a statistical analysis allows to predict, for instance, the behavior of the RF circuit response with the presence of design uncertainties. Typical characterizations of such random quantities include the estimation of their expected (average) value, standard deviation and probability density function (pdf) [23]. This chapter introduces the basic concepts of stochastic analysis and illustrates the traditional MC method, followed by the more recent approach based on Polynomial Chaos.

3.1 Notations and Preliminaries of Statistical Analysis

3.1.1 Formulation of HB with Design Uncertainty

MNA formulation of general nonlinear circuit in time domain with d uncertain design parameters denoted by $\boldsymbol{\xi} = [\xi_1, \xi_2, \cdots, \xi_d]$ is typically formulated as follows,

$$\boldsymbol{C}\frac{d\boldsymbol{x}(t,\boldsymbol{\xi})}{dt} + \boldsymbol{G}\boldsymbol{x}(t,\boldsymbol{\xi}) + \boldsymbol{f}(\boldsymbol{x}(t,\boldsymbol{\xi}),\boldsymbol{\xi}) = \boldsymbol{b}(t) \tag{3.1}$$

where, $\boldsymbol{x}(t,\boldsymbol{\xi}) \in \mathbb{R}^N$ is a vector of node voltages, appended by currents in inductors and independent voltage sources, $\boldsymbol{f}(\boldsymbol{x}(t,\boldsymbol{\xi})$ is a vector representing, the nonlinear elements, $\boldsymbol{b}(t) \in \mathbb{R}^N$ is a vector representing the independent stimuli, and N is the size of the MNA formulation.

In the context of RF integrated circuits, the circuit is typically excited by a set of W independent tones $\omega_i, (i = 1, \cdots, W)$ and the objective is to compute its quasi-periodic steady-state [19]. The HB approach used to achieve this objective first expands all t-dependent quantities in (3.1) as a generalized Fourier series, with say H terms, whose coefficients become $\boldsymbol{\xi}$-dependent, thereby leading to a nonlinear algebraic system of the form

$$\boldsymbol{Y}\bar{\boldsymbol{X}}(\boldsymbol{\xi}) + \bar{\boldsymbol{F}}\left(\bar{\boldsymbol{X}}(\boldsymbol{\xi}),\boldsymbol{\xi}\right) = \bar{\boldsymbol{B}} \tag{3.2}$$

where $\bar{\boldsymbol{X}}(\boldsymbol{\xi})$, and $\bar{\boldsymbol{B}} \in \mathbb{R}^{NH}$ are vectors containing the Fourier coefficients of $\boldsymbol{x}(t,\boldsymbol{\xi})$ and $\boldsymbol{b}(t)$, respectively, whereas $\bar{\boldsymbol{F}}\left(\bar{\boldsymbol{X}}(\boldsymbol{\xi}),\boldsymbol{\xi}\right)$ can be described succinctly with the help of the Kronecker operator $\otimes$ as follows,

$$\bar{\boldsymbol{F}} = \bar{\boldsymbol{\Gamma}}\sum_{k=1}^{H}\boldsymbol{f}\left(\boldsymbol{x}_k(\boldsymbol{\xi}),\boldsymbol{\xi}\right) \otimes \mathbf{e}_{k,H}, \tag{3.3}$$

with $\boldsymbol{x}_k(\boldsymbol{\xi}) \in \mathbb{R}^N$ given by

$$\boldsymbol{x}_k(\boldsymbol{\xi}) = (\mathbf{I}_N \otimes \mathbf{e}_{k,H}^{\top})(\bar{\boldsymbol{\Gamma}}^{-1}\bar{\boldsymbol{X}}(\boldsymbol{\xi})) \tag{3.4}$$

where, $\mathbf{I}_N$ is an identity matrix of size $N \times N$. Different methods can be employed in order to analyse the uncertain HB response, with the most commonly used method is based on MC simulations that will be described next.

3.2 Monte Carlo Analysis

The traditional approach to accomplish the variability analysis of HB response in RF circuits, is based on the MC simulation, which proceeds by repeatedly computing the steady state response $\bar{\boldsymbol{X}}(\boldsymbol{\xi})$ by solving (3.2), for randomly selected points in the d-dimensional space spanned by the vector $\boldsymbol{\xi}$. Finally, the MC terminates if the computed *statistical* moments (e.g. mean or standard deviation) converge to fixed values. Upon solving the above problem for $i = 1, 2, \cdots, K$, statistical information such as mean and variance can be extracted by the following estimators

$$\mu_{\bar{\boldsymbol{X}}} = E\{\boldsymbol{X}\} \approx \hat{\mu}_{\bar{\boldsymbol{X}}} = \frac{1}{K}\sum_{i=1}^{K} \bar{\boldsymbol{X}}_i \tag{3.5}$$

$$\sigma^2_{\bar{\boldsymbol{X}}} = var(\bar{\boldsymbol{X}}) \approx \hat{\sigma}^2_{\bar{\boldsymbol{X}}} = \frac{1}{K-1}\sum_{i=1}^{K} (\bar{\boldsymbol{X}}_i - \hat{\mu}_{\bar{\boldsymbol{X}}})^2 \tag{3.6}$$

where K denotes the number of MC simulations. Although MC has been traditionally used to obtain the statistical information of circuit performance metrics, such as the IIP3, its significant computation cost due to the slow convergence has become the major disadvantage of this method. For example, mean value typically converges at the rate of $\frac{1}{\sqrt{K}}$.

3.3 Generalized Polynomial Chaos (gPC)

3.3.1 Preliminaries of PC-based Variability Analysis

The underlying idea of PC is to represent stochastic solutions in terms of orthogonal polynomial expansions of the random design parameters. In the first applications of PC, Hermite polynomials were employed as an orthogonal basis to represent random processes, however, for Non-Gaussian problems, more suitable polynomial bases can be chosen, according to the probability distribution of the random inputs. The choice, yielding optimal convergence, follows the so-called Askey scheme, and defines the generalized polynomial chaos framework. Table 3.1 illustrates different type of gPC basis and their appropriate supports and distributions.

Table 3.1: Wiener-Askey Polynomial Chaos.

Distribution of $\boldsymbol{\xi}$	Class of orthogonal polynomials polynomial	Support
Uniform	Legendre	$[a, b]$
Gaussian	Hermite	$(-\infty, \infty)$
Gamma	Laguerre	$[0, \infty)$
Beta	Jacobi	$[a, b]$

The PC approach to quantifying the uncertainties associated with circuits response $\bar{\boldsymbol{X}}(\boldsymbol{\xi})$ is

based on expanding it in a series of the form,

$$\bar{\boldsymbol{X}}(\boldsymbol{\xi}) \approx \sum_{\boldsymbol{\alpha}\in\Upsilon_M} \boldsymbol{\mathcal{X}}_{\boldsymbol{\alpha}}\phi_{\boldsymbol{\alpha}}(\boldsymbol{\xi}), \tag{3.7}$$

where $\boldsymbol{\mathcal{X}}_{\boldsymbol{\alpha}} \in \mathbb{R}^{NH}$ are the series coefficients, $\phi(\boldsymbol{\xi})$ is a set of multi-dimensional polynomials that are orthogonal with respect to a probability density function $w(\boldsymbol{\xi})$ with support on χ, and the summation is over all the elements in Υ_M. The orthogonality implies that

$$\langle\phi_{\boldsymbol{\alpha}}(\boldsymbol{\xi}), \phi_{\boldsymbol{\beta}}(\boldsymbol{\xi})\rangle = \int_{\chi} \phi_{\boldsymbol{\alpha}}(\boldsymbol{\xi})\phi_{\boldsymbol{\beta}}(\boldsymbol{\xi})w(\boldsymbol{\xi})\mathrm{d}\boldsymbol{\xi} = \zeta_{\boldsymbol{\alpha}}\delta_{\boldsymbol{\alpha}\boldsymbol{\beta}}, \tag{3.8}$$

with $\delta_{\boldsymbol{\alpha}\boldsymbol{\beta}} = \prod_{i=1}^{d} \delta_{\alpha_i\beta_i}$, δ_{mn} being the Kronecker delta function and

$$\zeta_{\boldsymbol{\alpha}} = \int_{\chi} \phi_{\boldsymbol{\alpha}}(\boldsymbol{\xi})\phi_{\boldsymbol{\alpha}}(\boldsymbol{\xi})w(\boldsymbol{\xi})\mathrm{d}\boldsymbol{\xi}. \tag{3.9}$$

is the normalization factor being. If the joint probability density function (pdf) of $\boldsymbol{\xi}$ is one of the standard distributions (e.g. Gaussian, Uniform, or Beta) the optimal basis functions are of the Askey-Wiener type (i.e. Hermite, Legendre, or Laguerre) which are orthogonal with respect to the weighting function given by the pdf [12].

In the PC framework, the polynomials of the Askey-Wiener scheme are optimal for the corresponding distribution. This means that, in theory, their PC expansion converges at an exponential rate [24]. The main focus of this paper is on random variables modelled by Gaussian and uniform PDF, and therefore the orthogonal polynomials adopted in this work are the Hermite and Legendre polynomials. Taking that $\phi_p(\xi)$, with p being an integer, as the single-dimensional probabilist's PC polynomial and choosing a maximum degree p, the elements of the multivariate basis $\phi_{\boldsymbol{\alpha}}(\boldsymbol{\xi})$ can be readily obtained as products of a sequence of univariate polynomials in each direction as follows [25] ,

$$\phi_{\boldsymbol{\alpha}}(\boldsymbol{\xi}) = \prod_{i=1}^{d} \phi_{\alpha_i}(\xi_i), \tag{3.10}$$

- **Sets of Multi-Indices** A common task often associated with the notion of multi-index is defining and ordering a finite set of multi-indices. One of the approaches for defining a set of multi-indices is based on the notion of tensor order [14] which defines a set Υ_M of multi-indices $\boldsymbol{\alpha}$ where $\Upsilon_M := \{\boldsymbol{\alpha} : \alpha_i \leq p\}$ and $M = \Pi_{i=1}^{d}(p+1)$. Table.3.2 illustrates the multi-index of Hermaite Polynomials considering two Gaussian Random Variables, in this table, $|\boldsymbol{\alpha}|$ is denoted as the rank of multi-indices $\boldsymbol{\alpha}$.

Table 3.2: multi-dimensional PC with $d = 2$, $M_1 = M_2 = 2$ (the distribution of two random variables are Gaussian

α_1	α_2	$\lvert\boldsymbol{\alpha}\rvert$	$\phi_{\boldsymbol{\alpha}}$	Polynomials
0	0	0	$H_0(\xi_1)H_0(\xi_2)$	1
0	1	1	$H_0(\xi_1)H_1(\xi_2)$	ξ_2
0	2	2	$H_0(\xi_1)H_2(\xi_2)$	$(\xi_2^2 - 1)$
1	0	3	$H_1(\xi_1)H_0(\xi_2)$	ξ_1
1	1	4	$H_1(\xi_1)H_1(\xi_2)$	$\xi_1\xi_2$
1	2	5	$H_1(\xi_1)H_2(\xi_2)$	$\xi_1(\xi_2^2 - 1)$
2	0	6	$H_2(\xi_1)H_0(\xi_2)$	$\xi_1^2 - 1$
2	1	7	$H_2(\xi_1)H_1(\xi_2)$	$(\xi_1^2 - 1)\xi_2$
2	2	8	$H_2(\xi_1)H_2(\xi_2)$	$(\xi_1^2 - 1)(\xi_2^2 - 1)$

3.4 Computation of gPC Coefficient

The core computation of gPC approach is computing the coefficient $\boldsymbol{\mathcal{X}}$. These coefficients are computed first by projecting $\bar{\boldsymbol{X}}(\boldsymbol{\xi})$ in the polynomial space, i.e, by performing the inner product $\left\langle \bar{\boldsymbol{X}}(\boldsymbol{\xi}), \phi_\alpha(\boldsymbol{\xi}) \right\rangle$ which reduces (due to the orthogonality property of $\phi_{\boldsymbol{\alpha}}$) to

$$\left\langle \bar{\boldsymbol{X}}(\boldsymbol{\xi}), \phi_\alpha(\boldsymbol{\xi}) \right\rangle = \left\langle \sum_{\boldsymbol{\beta}} \boldsymbol{\mathcal{X}}_{\boldsymbol{\beta}} \phi_{\boldsymbol{\beta}}(\boldsymbol{\xi}), \phi_{\boldsymbol{\alpha}}(\boldsymbol{\xi}) \right\rangle = \int_\chi \sum_{\boldsymbol{\beta}} \boldsymbol{\mathcal{X}}_{\boldsymbol{\beta}} \phi_{\boldsymbol{\beta}}(\boldsymbol{\xi}) \phi_{\boldsymbol{\alpha}}(\boldsymbol{\xi}) w(\boldsymbol{\xi}) \partial \boldsymbol{\xi} \tag{3.11}$$

and by utilizing (3.9), thereby enabling the extraction of the coefficients $\boldsymbol{\mathcal{X}}$ as follows,

$$\boldsymbol{\mathcal{X}}_{\boldsymbol{\alpha}} = \frac{\left\langle \bar{\boldsymbol{X}}(\boldsymbol{\xi}), \phi_{\boldsymbol{\alpha}}(\boldsymbol{\xi}) \right\rangle}{\left\langle \phi_{\boldsymbol{\alpha}}(\boldsymbol{\xi}), \phi_{\boldsymbol{\alpha}}(\boldsymbol{\xi}) \right\rangle} = \frac{\int_\chi \bar{\boldsymbol{X}}(\boldsymbol{\xi}) \phi_{\boldsymbol{\alpha}}(\boldsymbol{\xi}) w(\boldsymbol{\xi}) \partial \boldsymbol{\xi}}{\zeta_\alpha} = \frac{\int_\chi \sum_{\boldsymbol{\beta}} \boldsymbol{\mathcal{X}}_{\boldsymbol{\beta}} \phi_{\boldsymbol{\beta}}(\boldsymbol{\xi}) \phi_{\boldsymbol{\alpha}}(\boldsymbol{\xi}) w(\boldsymbol{\xi}) \partial \boldsymbol{\xi}}{\zeta_\alpha} \tag{3.12}$$

As can be seen from above equation, using the above projection techniques requires a prior knowledge of $\bar{\boldsymbol{X}}(\boldsymbol{\xi})$ to perform the inner product. In order to achieve that computation, two approach are typically followed, namely the Stochastic Collocation (SC) and Stochastic Galerkin Projection (GP) methods. Those approaches are presented next.

3.4.1 Stochastic Collocation Method

Stochastic Collocation approaches (SC) such as Pseudo Spectral Approach and matrix inversion methods aiming to extract the coefficients $\boldsymbol{\mathcal{X}}_\alpha$, rely on solving equation (3.2) for N_s collocation points, i .e, $\boldsymbol{\xi}^i = [\boldsymbol{\xi}^1 \cdot \cdot \boldsymbol{\xi}^{N_s}]^T$ in order to obtain $\bar{\boldsymbol{X}}(\boldsymbol{\xi}^i) = [\bar{\boldsymbol{X}}(\boldsymbol{\xi}^1) \cdot \cdot \bar{\boldsymbol{X}}(\boldsymbol{\xi}^{N_s})]^T$. In this section both methods are summarized.

Pseudo Spectral Approach

In this method, (3.2) is deterministic for each $\boldsymbol{\xi}^i$, hence, SC involves solving N_s deterministic systems. In Pseudo Spectral Approach, the gPC coefficient $\boldsymbol{\mathcal{X}}_\alpha$ are computed through substituting $\bar{\boldsymbol{X}}(\boldsymbol{\xi}^i)$ in following equation,

$$\boldsymbol{\mathcal{X}}_\alpha = \langle \bar{\boldsymbol{X}}(\boldsymbol{\xi}^N), \boldsymbol{\phi}_\alpha(\boldsymbol{\xi}^N) \rangle \approx \sum_{i=1}^{Ns} \bar{\boldsymbol{X}}(\xi^i)\phi_{\boldsymbol{\alpha}}(\xi^i)w^i, \tag{3.13}$$

In the above equation, $\boldsymbol{\xi}_i$ are collocation points and $w_i = [w^1 \cdot \cdot w^{N_s}]^T$ are weights that need to be obtained via either proper quadrature Tensor Product rule or Sparse Grid method [26] with respect to their distribution type.

Matrix Inversion Approach

The Matrix Inversion approach aims to find an approximation, $\bar{\boldsymbol{Z}}(\boldsymbol{\xi})$ in order to approximate the actual response, $\bar{\boldsymbol{X}}(\boldsymbol{\xi})$ of the circuit, where the approximation is the same as $\bar{\boldsymbol{X}}(\boldsymbol{\xi})$ at a discrete set of N_s nodes (collocation points) $\boldsymbol{\xi}^i$ $i = 1, 2, \cdots, N_s$, i.e.,

$$\bar{\boldsymbol{Z}}(\boldsymbol{\xi}^i) \equiv \bar{\boldsymbol{X}}(\boldsymbol{\xi}^i) \tag{3.14}$$

This approach starts by defining a polynomial interpolating basis, such as,

$$\bar{\boldsymbol{Z}}(\boldsymbol{\xi}) = \sum_{\boldsymbol{\alpha} \in \Upsilon_M} \boldsymbol{\mathcal{Z}}_{\boldsymbol{\alpha}} \phi_{\boldsymbol{\alpha}}(\boldsymbol{\xi}), \tag{3.15}$$

Here, expansion coefficients $\boldsymbol{\mathcal{Z}}_{\boldsymbol{\alpha}}$ are used to approximate gPC coefficients $\boldsymbol{\mathcal{X}}_{\boldsymbol{\alpha}}$ in (3.7). It is shown in [26] that (3.15) can be written into a matrix form of,

$$(\boldsymbol{A} \otimes I_N)\overline{\boldsymbol{\mathcal{Z}}} = \bar{\boldsymbol{X}}(\boldsymbol{\xi}^i), \tag{3.16}$$

where $\bar{\boldsymbol{X}}(\boldsymbol{\xi}^i) = [\bar{\boldsymbol{X}}(\boldsymbol{\xi}^1) \cdot \cdot \bar{\boldsymbol{X}}(\boldsymbol{\xi}^{N_s})]^T$ and $\overline{\boldsymbol{\mathcal{Z}}}$ is a vector constructed from the expansion coefficients $\boldsymbol{\mathcal{Z}}_{\boldsymbol{\alpha}}$ and $\boldsymbol{A}$ is a $N_s \times M$ matrix in the following form,

$$[\boldsymbol{A}]_{i,j} = \phi_{\boldsymbol{\alpha}}(\boldsymbol{\xi}_i), \quad |\boldsymbol{\alpha}| = j - 1, \tag{3.17}$$

It is important here to stress that in this approach $N_s \geq M$ to prevent problem become underdetermined.

Although Stochastic Collocation methods are conceptually straightforward and easy to implement, however, SC requires a large number of collocation points analysing higher dimensional random spaces that causes a significant computational cost. In addition to the computational cost, the aliasing errors is another concern in stochastic collocation approaches, especially, for higher dimensional random spaces [26].

3.4.2 Stochastic Galerkin Projection Method

Another approach uses the Galerkin projection (GP), which proceeds by expanding the $\boldsymbol{\xi}$-dependent terms in (3.2) in a series similar to (3.7) with gPC basis function,

$$\bar{\boldsymbol{F}}\left(\bar{\boldsymbol{X}}(\boldsymbol{\xi}), \boldsymbol{\xi}\right) = \sum_{\boldsymbol{\beta} \in \Upsilon_M} \boldsymbol{\mathcal{F}}_{\boldsymbol{\beta}}\left(\overline{\boldsymbol{\mathcal{X}}}\right) \phi_{\boldsymbol{\beta}}(\boldsymbol{\xi}) \tag{3.18}$$

$$\boldsymbol{Y} = \sum_{\boldsymbol{\beta} \in \Upsilon_M} \boldsymbol{\mathcal{Y}}_{\boldsymbol{\beta}} \phi_{\boldsymbol{\beta}}(\boldsymbol{\xi}) \tag{3.19}$$

where $\overline{\boldsymbol{\mathcal{X}}} \in \mathbb{R}^{NHM}$ is a vector that consists of the gPC coefficients $\boldsymbol{\mathcal{X}}_{\boldsymbol{\alpha}}$ of $\bar{\boldsymbol{X}}(\boldsymbol{\xi})$, while $\boldsymbol{\mathcal{F}}_{\boldsymbol{\beta}}$ and $\boldsymbol{\mathcal{Y}}_{\boldsymbol{\beta}}$ are the gPC coefficients of $\bar{\boldsymbol{F}}$ and $\boldsymbol{Y}$, respectively, which depend on $\overline{\boldsymbol{\mathcal{X}}}$. The GP next substitutes from (3.19) and (3.18) into (3.2) and utilizes the orthogonality property of $\phi_{\boldsymbol{\beta}}(\boldsymbol{\xi})$ to eliminate $\boldsymbol{\xi}$ from (3.2). This process is actually carried out by multiplying by $\phi_{\boldsymbol{\gamma}}(\boldsymbol{\xi})$, integrating

over χ and then repeating the process for all possible $\boldsymbol{\gamma} \in \Upsilon_M$ and by using the notion of Triple Product Integral as,

$$\boldsymbol{\Psi}_{\boldsymbol{\beta},\boldsymbol{\alpha},\boldsymbol{\gamma}} = \int_{\boldsymbol{\chi}} \phi_{\boldsymbol{\beta}}(\boldsymbol{\xi})\phi_{\boldsymbol{\alpha}}(\boldsymbol{\xi})\phi_{\boldsymbol{\gamma}}(\boldsymbol{\xi})\boldsymbol{w}(\boldsymbol{\xi})d\boldsymbol{\xi} = \prod_{i=1}^{d} \Psi_{\beta_i,\alpha_i,\gamma_i} \tag{3.20}$$

where, $\Psi_{\beta_i,\alpha_i,\gamma_i} = \int_{\chi_i} \phi_{\beta_i}(\xi_i)\phi_{\alpha_i}(\xi_i)\phi_{\gamma_i}(\xi_i)w_i(\xi_i)d\xi_i$. This process results in a new larger system of nonlinear equations, which can be represented compactly using

$$\overline{\boldsymbol{\mathcal{Y}}}\,\overline{\boldsymbol{\mathcal{X}}} + \overline{\boldsymbol{\mathcal{F}}}(\overline{\boldsymbol{\mathcal{X}}}) = \overline{\boldsymbol{\mathcal{B}}} \tag{3.21}$$

where,$\overline{\boldsymbol{\mathcal{X}}}$, $\overline{\boldsymbol{\mathcal{F}}}$ and $\overline{\boldsymbol{\mathcal{Y}}}$ are vectors and matrices consist, respectively, of the Hermite coefficients $\boldsymbol{\mathcal{X}}_{\boldsymbol{\beta}}, \boldsymbol{F}_{\boldsymbol{\beta}}, \boldsymbol{\mathcal{Y}}_{\boldsymbol{\beta}} \forall \boldsymbol{\beta} \in \Upsilon_M$, and $\overline{\boldsymbol{\mathcal{B}}}$ is a vector that has $\bar{\boldsymbol{U}}$ in the first NH entries, and zeros otherwise.

The key advantage of the PC-based variability analysis is that, once the coefficients $\boldsymbol{\mathcal{X}}_{\boldsymbol{\alpha}}$ are computed, through solving (3.21), then computing the statistical properties of the stochastic process $\bar{\boldsymbol{X}}(\boldsymbol{\xi})$, (e.g. mean $\boldsymbol{E}[\bar{\boldsymbol{X}}(\boldsymbol{\xi})]$ and variance $var[\bar{\boldsymbol{X}}(\boldsymbol{\xi})]$), can be done analytically through these coefficients [12] as follows,

$$\boldsymbol{E}[\bar{\boldsymbol{X}}(\boldsymbol{\xi})] \approx \sum_{k=0}^{p} \boldsymbol{\mathcal{X}}_k \int_{\chi} \phi_{\boldsymbol{\alpha}}(\boldsymbol{\xi})w(\boldsymbol{\xi}) = \boldsymbol{\mathcal{X}}_0\zeta_0 \tag{3.22}$$

$$var[\bar{\boldsymbol{X}}(\boldsymbol{\xi})] \approx \int_{\chi} \bar{\boldsymbol{X}}^2(\boldsymbol{\xi})w(\boldsymbol{\xi})\partial\boldsymbol{\xi} - \boldsymbol{E}[\bar{\boldsymbol{X}}(\boldsymbol{\xi})]^2 = \sum_{k=1}^{p} \boldsymbol{\mathcal{X}}_k\zeta_k^2 \tag{3.23}$$

The PC approach, therefore, does not suffer from the convergence difficulties encountered in the MC-based approaches.

3.4.3 Difficulties In Standard gPC Approach

The main drawback in the standard gPC approach in statistical analysis of steady state response in RF circuits arises from the numerical difficulty of solving the nonlinear computational problem (3.21) to compute the coefficients $\boldsymbol{\mathcal{X}}_{\alpha}$, which requires factorizing the corresponding Jacobian matrix, henceforth denoted by $\boldsymbol{\mathcal{J}}_{\text{HB-PC}}$. In fact, the main computational difficulty in this step is caused by the large size and the dense structure of this matrix. Nevertheless, it is typically the dense structure of this matrix that makes factorizing it very difficult even for medium sized circuits; often times beyond the capabilities of typical computing systems. In the following sections, we propose a new approach to address this issue. The illustration of the proposed approach will be carried out in two steps. The first step, presented in the following section, will derive a closed-form analytical formula describing the structure of $\boldsymbol{\mathcal{J}}_{\text{HB-PC}}$ and revealing its key structural properties. The second step, builds on this formula to decouple this matrix into smaller matrices that can be factorized independently with much greater efficiency.

Chapter 4

Computationally Efficient Decoupled Approach in HB-PC Analysis

In previous chapter Stochastic Galerkin method in order to statistically analyse the steady state response of RF circuits was presented. However, it still does not bring concrete computational savings in actual implementation. In this chapter an efficient method will be introduced that efficiently decouples the large and dense Jacobian matrix of gPC method into a block diagonal matrix consisting of smaller matrices that can be factorized independently and consequently reduce the computation cost and memory usage. First, a closed form for $\mathcal{J}_{\text{HB-PC}}$ will be presented that lead us to interesting properties that can be used in proposed decoupled method. Next, the fundamental of proposed approach will be described for both single and multi-random variables. For simplicity Hermite Polynomials have been used in this chapter, however, the method is general and can be used for variety of different types of Askey-Wiener Polynomials .

4.1 Development of Closed-Form Description for $\mathcal{J}_{\text{HB-PC}}$

Let the jacobian matrix $\bar{\boldsymbol{J}}(\boldsymbol{x}, \boldsymbol{\xi})$ and matrix $\boldsymbol{Y}$ from (3.2), be described by a Hermite expansion,

$$\bar{\boldsymbol{J}}(\boldsymbol{x}_k(\boldsymbol{\xi}), \boldsymbol{\xi}) = \sum_{\beta \in \Upsilon_M} \boldsymbol{\mathcal{J}}_{\boldsymbol{\beta}}^{(k)} \mathcal{H}_{\boldsymbol{\beta}}(\boldsymbol{\xi}) \tag{4.1}$$

$$\boldsymbol{Y} = \sum_{\beta \in \Upsilon_M} \boldsymbol{\mathcal{Y}}_{\boldsymbol{\beta}}^{(k)} \mathcal{H}_{\boldsymbol{\beta}}(\boldsymbol{\xi}) \tag{4.2}$$

where $\boldsymbol{\mathcal{J}}_{\boldsymbol{\beta}}^{(k)}$ and $\boldsymbol{\mathcal{Y}}_{\boldsymbol{\beta}}^{(k)} \in \mathbb{R}^{N \times N}$ are the (matrix-valued) Hermite coefficients of $\boldsymbol{J}(\boldsymbol{x}_k(\boldsymbol{\xi}), \boldsymbol{\xi})$ and $\boldsymbol{Y}$, respectively.

Furthermore, define the matrices $\overline{\boldsymbol{\mathcal{J}}}_{\boldsymbol{\beta}}, \overline{\boldsymbol{\mathcal{Y}}}_{\boldsymbol{\beta}} \in \mathbb{R}^{NG \times NG}$ as follows

$$\overline{\boldsymbol{\mathcal{J}}}_{\boldsymbol{\beta}} = \bar{\boldsymbol{\Gamma}} \left(\sum_{k=1}^{G} \boldsymbol{\mathcal{J}}_{\boldsymbol{\beta}}^{(k)} \otimes \mathbf{e}_{k,G} \mathbf{e}_{k,G}^{\top} \right) \bar{\boldsymbol{\Gamma}}^{-1} \tag{4.3}$$

It is important to remark at this point that both of $\overline{\boldsymbol{\mathcal{J}}}_{\boldsymbol{\beta}}$ and $\overline{\boldsymbol{\mathcal{Y}}}_{\boldsymbol{\beta}}$, have identical structures as that of $\bar{\boldsymbol{J}}_Q$ and $\bar{\boldsymbol{Y}}$ of (2.10), i.e., they have the same size and the same pattern of nonzero entries.

Next, we will first describe the main result of this section for the special case of a single random variable ($d = 1$) in Subsection 4.1.1. The generalization to multi-random variables will follow in Subsection 4.1.2.

4.1.1 $\mathcal{J}_{\text{HB-PC}}$ for Single Random Variable ($d = 1$)

For a single random variable ξ, $d = 1$, the Hermite expansions in (3.7), (3.19) and (3.18) can be expressed in the classical scalar index format, whereby the multi-index $\boldsymbol{\alpha}$ is replaced by scalar index, $p \in \mathbb{N}$, the summation over Υ_M is replaced by a summation over $p = 0, \cdots, P_1$, and M (the size of Υ_M) reduces to P_1, (i.e. $M = P_1$). In addition, the multi-dimensional $\mathcal{H}(\boldsymbol{\xi})$ is

replaced by the single dimensional $H_p(\xi)$. Thus (3.7), (3.18), and (3.19) become,

$$\bar{\boldsymbol{X}}(\xi) = \sum_{p=0}^{M-1} \boldsymbol{\mathcal{X}}_p H_p(\xi), \tag{4.4}$$

$$\bar{\boldsymbol{F}}(\bar{\boldsymbol{X}}(\xi), \xi) = \sum_{p=0}^{M-1} \boldsymbol{\mathcal{F}}_p \left(\overline{\boldsymbol{\mathcal{X}}}\right) H_p(\xi), \tag{4.5}$$

$$\bar{\boldsymbol{Y}} = \sum_{p=0}^{M-1} \boldsymbol{\mathcal{Y}}_p H_p(\xi), \tag{4.6}$$

Likewise, (4.1) can be reproduced by,

$$\bar{\boldsymbol{J}}(\boldsymbol{x}_k(\boldsymbol{\xi}), \boldsymbol{\xi}) = \sum_{p=0}^{M-1} \boldsymbol{\mathcal{J}}_p^{(k)} H_p(\xi) \tag{4.7}$$

The following theorem describes the structure of $\boldsymbol{\mathcal{J}}_{\text{HB-PC}}$ for the single random variable case. First, we present the basis matrix used in the theorem, $\boldsymbol{K}_{p,M}$.

Denoted by $\boldsymbol{K}_{p,M} \in \mathbb{R}^{M\times M}$ the matrix whose (row,column) $(m+1, n+1)$ entry $((0,0) \leq (m,n) \leq (M-1, M-1))$ is given by $\theta_{m,n,p}$, where

$$\theta_{m,n,p} = \frac{1}{\sqrt{2\pi} m!} \int_{-\infty}^{\infty} H_m(\xi) H_n(\xi) H_p(\xi) e^{\frac{-||\xi||^2}{2}} \mathrm{d}\xi, \tag{4.8}$$

i.e.,

$$\boldsymbol{K}_{p,M} = \left[\theta_{m,n,p}\right]_{m,n=0}^{m,n=M-1} \tag{4.9}$$

Theorem 1. *For the case of a single random variable $d = 1$, $\boldsymbol{\mathcal{J}}_{\text{HB-PC}}$ can be expressed as follows,*

$$\boldsymbol{\mathcal{J}}_{\text{HB-PC}} = \sum_{p=0}^{M-1} \boldsymbol{K}_{p,M} \otimes \overline{\boldsymbol{\mathcal{J}}}_p + \sum_{p=0}^{M-1} \boldsymbol{K}_{p,M} \otimes \overline{\boldsymbol{\mathcal{Y}}}_p \tag{4.10}$$

Proof. From (3.21), it is obvious that $\boldsymbol{\mathcal{J}}_{\text{HB-PC}}$ is given by

$$\boldsymbol{\mathcal{J}}_{\text{HB-PC}} = \frac{\partial \overline{\boldsymbol{\mathcal{F}}}}{\partial \overline{\boldsymbol{\mathcal{X}}}} + \overline{\boldsymbol{\mathcal{Y}}} \tag{4.11}$$

where,

$$\frac{\partial \overline{\boldsymbol{\mathcal{F}}}}{\partial \overline{\boldsymbol{\mathcal{X}}}} = \left[\frac{\partial \boldsymbol{\mathcal{F}}_m}{\partial \boldsymbol{\mathcal{X}}_n}\right]_{m,n=0}^{m,n=M-1}, \tag{4.12}$$

Nonetheless, applying the orthogonality property of the Hermite polynomials on (4.6) and (4.5) shows that

$$\boldsymbol{\mathcal{F}}_m = \frac{1}{\sqrt{2\pi m!}} \int_{-\infty}^{\infty} \bar{\boldsymbol{F}}\left(\bar{\boldsymbol{X}}(\xi), \xi\right) H_m(\xi) e^{\frac{-||\xi||^2}{2}} \mathrm{d}\xi \tag{4.13}$$

$$\boldsymbol{\mathcal{Y}}_m = \frac{1}{\sqrt{2\pi m!}} \int_{-\infty}^{\infty} \bar{\boldsymbol{Y}}(\xi) H_m(\xi) e^{\frac{-||\xi||^2}{2}} \mathrm{d}\xi \tag{4.14}$$

Differentiating both sides of (4.13) with respect to $\boldsymbol{\mathcal{X}}_n$, we proceed with the following manipulations,

$$\begin{aligned}
\frac{\partial \boldsymbol{\mathcal{F}}_m}{\partial \boldsymbol{\mathcal{X}}_n} &= \int_{-\infty}^{\infty} \frac{\partial \bar{\boldsymbol{F}}\left(\bar{\boldsymbol{X}}(\xi), \xi\right)}{\partial \boldsymbol{\mathcal{X}}_n} \frac{H_m(\xi)}{\sqrt{2\pi m!}} e^{\frac{-||\xi||^2}{2}} \mathrm{d}\xi \\
&= \int_{-\infty}^{\infty} \frac{\partial \bar{\boldsymbol{F}}\left(\bar{\boldsymbol{X}}(\xi), \xi\right)}{\partial \bar{\boldsymbol{X}}} \frac{\partial \bar{\boldsymbol{X}}(\xi)}{\partial \boldsymbol{\mathcal{X}}_n} \frac{H_m(\xi)}{\sqrt{2\pi m!}} e^{\frac{-||\xi||^2}{2}} \mathrm{d}\xi \\
&= \int_{-\infty}^{\infty} \frac{\partial \bar{\boldsymbol{F}}\left(\bar{\boldsymbol{X}}(\xi), \xi\right)}{\partial \bar{\boldsymbol{X}}} H_n(\xi) \frac{H_m(\xi)}{\sqrt{2\pi m!}} e^{\frac{-||\xi||^2}{2}} \mathrm{d}\xi \\
&= \int_{-\infty}^{\infty} \bar{\boldsymbol{\Gamma}} \sum_{k=1}^{G} \boldsymbol{J}(\boldsymbol{x}, \boldsymbol{\xi})|_{\boldsymbol{x}=\boldsymbol{x}_k} \otimes \mathbf{e}_{k,G} \frac{\partial \boldsymbol{x}_k}{\partial \bar{\boldsymbol{X}}} \frac{H_m(\xi)}{\sqrt{2\pi m!}} H_n(\xi) e^{\frac{-||\xi||^2}{2}} \mathrm{d}\xi \\
&= \int_{-\infty}^{\infty} \bar{\boldsymbol{\Gamma}} \sum_{k=1}^{G} \left(\boldsymbol{J}(\boldsymbol{x}_k(\boldsymbol{\xi}), \boldsymbol{\xi}) \otimes \mathbf{e}_{k,G}\right) \left(\mathbf{I}_N \otimes \mathbf{e}_{k,G}^{\top}\right) \bar{\boldsymbol{\Gamma}}^{-1} \\
&\qquad\qquad H_n(\xi) \frac{H_m(\xi)}{\sqrt{2\pi m!}} e^{\frac{-||\xi||^2}{2}} \mathrm{d}\xi \\
&= \int_{-\infty}^{\infty} \bar{\boldsymbol{\Gamma}} \sum_{k=1}^{G} \boldsymbol{J}(\boldsymbol{x}_k(\boldsymbol{\xi}), \boldsymbol{\xi}) \otimes \left(\mathbf{e}_{k,G} \mathbf{e}_{k,G}^{\top}\right) \bar{\boldsymbol{\Gamma}}^{-1} \\
&\qquad\qquad H_n(\xi) \frac{H_m(\xi)}{\sqrt{2\pi m!}} e^{\frac{-||\xi||^2}{2}} \mathrm{d}\xi \\
&= \sum_{p=0}^{M-1} \theta_{m,n,p} \bar{\boldsymbol{\Gamma}} \sum_{k=1}^{G} \boldsymbol{\mathcal{J}}_p^{(k)} \otimes \left(\mathbf{e}_{k,G} \mathbf{e}_{k,G}^{\top}\right) \bar{\boldsymbol{\Gamma}}^{-1} \\
&= \sum_{p=0}^{M-1} \theta_{m,n,p} \overline{\boldsymbol{\mathcal{J}}}_p
\end{aligned}$$

where, the equalities in the above manipulation are obtained as follows,

2nd **equality:** from applying the chain rule of differentiation,

3^{rd} **equality:** by employing (4.4),

4^{th} **equality:** from applying the chain rule of differentiation using (3.3),

5^{th} **equality:** from the definition of $\boldsymbol{x}_k(\boldsymbol{\xi})$ in (3.4)

6^{th} **equality:** by using the following property of the Kronecker product [27]

$$(\boldsymbol{A} \otimes \boldsymbol{B})\,(\boldsymbol{C} \otimes \boldsymbol{D}) = (\boldsymbol{AC}) \otimes (\boldsymbol{BD}) \tag{4.15}$$

7^{th} **equality:** by substituting from (4.7) for $\boldsymbol{J}$, and

8^{th} **equality:** through the utilization of the definitions of $\theta_{m,n,p}$ and $\overline{\mathcal{J}}_p$.

Finally, the Kronecker operator can be used, along with the definition of $\boldsymbol{K}_{p,M}$ to construct the full $\partial\overline{\boldsymbol{\mathcal{F}}}/\partial\overline{\boldsymbol{\mathcal{X}}}$, and $\overline{\boldsymbol{\mathcal{Y}}}$ matrices and prove the theorem. □

4.1.2 $\mathcal{J}_{\text{HB-PC}}$ for Multi-random Variables $(d > 1)$

Generalization of the result in Theorem 1 to the case of multi-random variables $\boldsymbol{\xi} \in \mathbb{R}^d$ requires first generalizing the terms used in this theorem. To this end, we define $\Theta_{\boldsymbol{\alpha},\boldsymbol{\beta},\boldsymbol{\gamma}}$ with multi-indices $\boldsymbol{\alpha}$, $\boldsymbol{\beta}$, and $\boldsymbol{\gamma}$ as a generalization of $\theta_{m,n,p}$ in (4.8) in the following sense

$$\Theta_{\boldsymbol{\alpha},\boldsymbol{\beta},\boldsymbol{\gamma}} = \int_{-\infty}^{\infty}\int_{-\infty}^{\infty}\cdots\int_{-\infty}^{\infty}\mathcal{H}_{\boldsymbol{\alpha}}(\boldsymbol{\xi})\mathcal{H}_{\boldsymbol{\beta}}(\boldsymbol{\xi})\mathcal{H}_{\boldsymbol{\gamma}}(\boldsymbol{\xi})e^{\frac{-||\boldsymbol{\xi}||^2}{2}}\mathrm{d}\boldsymbol{\xi} \tag{4.16}$$

where $\bar{\boldsymbol{\alpha}} = 1/\sqrt{2\pi}^d\prod_{i=1}^d \alpha_i!$. In an analogous manner, the matrix $\boldsymbol{\mathcal{K}}_{\boldsymbol{\gamma},M}$ ($\boldsymbol{\gamma}$ being a multi-index), is the generalization of $\boldsymbol{K}_{p,M}$ in (4.9) to the case of multi-random variables in the following way

$$\boldsymbol{\mathcal{K}}_{\boldsymbol{\gamma},M} = \left[\Theta_{\boldsymbol{\alpha},\boldsymbol{\beta},\boldsymbol{\gamma}}\right]_{\boldsymbol{\alpha},\boldsymbol{\beta}\in\boldsymbol{\Upsilon}_M} \tag{4.17}$$

It must be noted here that the size of the matrix $\boldsymbol{\mathcal{K}}_{\boldsymbol{\gamma},M}$ is $M \times M$. However, M in this case is the size of Υ_M (the set of multi-indices that are included in the series summation (3.7)), which is given $M = \Pi_{i=1}^{d} P_i$. Theorem 1 can, therefore, be generalized as follows.

Theorem 2. *For a circuit with d random parameters, $\boldsymbol{\xi}$, the matrix $\boldsymbol{\mathcal{J}}_{\text{HB-PC}}$ is given as follows,*

$$\boldsymbol{\mathcal{J}}_{\text{HB-PC}} = \sum_{\boldsymbol{\gamma} \in \Upsilon_M} \boldsymbol{\mathcal{K}}_{\boldsymbol{\gamma},M} \otimes \overline{\boldsymbol{\mathcal{J}}}_{\boldsymbol{\gamma}} + \sum_{\boldsymbol{\gamma} \in \Upsilon_M} \boldsymbol{\mathcal{K}}_{\boldsymbol{\gamma},M} \otimes \overline{\boldsymbol{\mathcal{Y}}}_{\boldsymbol{\gamma}} \tag{4.18}$$

Proof. The proof of this theorem can be carried out using analogous steps to those used in Theorem 1. For example, the partial derivative in (4.12) are now written as

$$\frac{\partial \overline{\boldsymbol{\mathcal{F}}}}{\partial \overline{\boldsymbol{\mathcal{X}}}} = \left[\frac{\partial \boldsymbol{\mathcal{F}}_{\boldsymbol{\alpha}}}{\partial \boldsymbol{\mathcal{X}}_{\boldsymbol{\beta}}} \right]_{\boldsymbol{\alpha},\boldsymbol{\beta} \in \Upsilon_M}, \tag{4.19}$$

Using a manipulation similar to the proof of Theorem 1, will lead to the following result,

$$\frac{\partial \boldsymbol{\mathcal{F}}_{\boldsymbol{\alpha}}}{\partial \boldsymbol{\mathcal{X}}_{\boldsymbol{\beta}}} = \sum_{\boldsymbol{\gamma} \in \Upsilon_M} \Theta_{\boldsymbol{\alpha},\boldsymbol{\beta},\boldsymbol{\gamma}} \bar{\boldsymbol{\Gamma}} \sum_{k=1}^{G} \boldsymbol{\mathcal{J}}_{\boldsymbol{\gamma}} \otimes \left(\mathbf{e}_{k,G} \mathbf{e}_{k,G}^{\top} \right) \bar{\boldsymbol{\Gamma}}^{-1} \tag{4.20}$$

$$\boldsymbol{\mathcal{Y}}_{\boldsymbol{\alpha}} = \sum_{\boldsymbol{\gamma} \in \Upsilon_M} \Theta_{\boldsymbol{\alpha},\boldsymbol{\beta},\boldsymbol{\gamma}} \boldsymbol{\mathcal{Y}}_{\boldsymbol{\gamma}} \tag{4.21}$$

Using the definitions of the Kronecker matrix product and the matrix in $\boldsymbol{\mathcal{K}}_{\boldsymbol{\gamma},M}$ in (5.34) proves the theorem. □

4.2 Preliminaries of Proposed Decoupled Method

The results of the previous section merely demonstrated that the Jacobian matrix of the HB-PC can be described in a compact closed-form analytical formula. However, it still does not bring concrete computational savings in actual implementation. Nonetheless, the insights provided by those results enable us to reformulate the problem in an alternative manner that produces

drastic reduction in the computational cost. The basic idea used to achieve this objective lies in analyzing the structure of the matrices $\boldsymbol{K}_{p,M}$ and $\boldsymbol{\mathcal{K}}_{\boldsymbol{\gamma},M}$. We begin by stating a powerful lemma [15, 28] used to characterize $\boldsymbol{K}_{p,M}$.

Lemma 1. *Let $\boldsymbol{K}_{0,M} = \mathbf{I}_M$. It then follows that $\boldsymbol{K}_{p,M}$ ($p > 0$) is given by*

$$\boldsymbol{K}_{p,M} = \boldsymbol{A}_L \boldsymbol{K}_{p-1,M} + \boldsymbol{K}_{p-1,M} \boldsymbol{A}_U \tag{4.22}$$

where,

$$\boldsymbol{A}_L = \begin{bmatrix} 0 & \cdots & & 0 \\ 1 & 0 & \cdots & 0 \\ 0 & 1 & 0 & \cdots \\ \vdots & \ddots & \cdots & 0 \\ 0 & \cdots & 1 & 0 \end{bmatrix}, \boldsymbol{A}_U = \begin{bmatrix} 0 & 1 & \cdots & & 0 \\ 0 & 0 & 2 & \cdots & 0 \\ 0 & 0 & 0 & 3 & \cdots \\ \vdots & \ddots & \cdots & 0 & M-1 \\ 0 & \cdots & \cdots & 0 & 0 \end{bmatrix}.$$

A direct corollary that follows immediately from the above lemma is that $\boldsymbol{K}_{p,M}$ can be written, using recursive substitution, as,

$$\boldsymbol{K}_{p,M} = \sum_{j=0}^{p} \frac{p!}{(p-j)!j!} \boldsymbol{A}_L^j \boldsymbol{A}_U^{p-j} \tag{4.23}$$

The key enabling point in the proposed approach is based on developing an alternative matrix, labelled $\tilde{\boldsymbol{K}}_{p,M}$, in place of $\boldsymbol{K}_{p,M}$, for constructing of $\boldsymbol{\mathcal{J}}_{\text{HB-PC}}$. $\tilde{\boldsymbol{K}}_{p,M}$ in this case is constructed as a matrix polynomial in the matrix $\boldsymbol{A}_L + \boldsymbol{A}_U$. To this end, we introduce $\psi_{p,M}(\lambda), \lambda \in \mathbb{R}$ as a polynomial in λ with a degree equal to p, and then use it to express the matrix $\tilde{\boldsymbol{K}}_{p,M}$ as matrix polynomial in the matrix $\boldsymbol{A}_L + \boldsymbol{A}_U$, i.e.,

$$\tilde{\boldsymbol{K}}_{p,M} = \psi_{p,M}\left(\boldsymbol{A}_L + \boldsymbol{A}_U\right) \tag{4.24}$$

$\tilde{\boldsymbol{K}}_{p,M}$ has two features that are pivotal in decoupling the structure of $\bar{\boldsymbol{\mathcal{J}}}_{HB-PC}$ into smaller matrices that can be factorized independently or in parallel on suitable platforms.

1. The first feature is that the matrix of eigenvectors of $\tilde{\boldsymbol{K}}_{p,M}$ is independent of p. This feature follows from the fact that $\tilde{\boldsymbol{K}}_{p,M}$ is a matrix polynomial of $\boldsymbol{A}_L + \boldsymbol{A}_U$ [29]. In other words, $\tilde{\boldsymbol{K}}_{p,M}$ can be written in the following eigen-decomposition from:

$$\tilde{\boldsymbol{K}}_{p,M} = \boldsymbol{V}_M \boldsymbol{\Psi}_{p,M}(\boldsymbol{\lambda}) \boldsymbol{V}_M^{-1} \tag{4.25}$$

   where $\boldsymbol{\Psi}_{p,M}(\boldsymbol{\lambda})$ is a diagonal matrix whose diagonal entries are given by $\psi_{p,M}(\lambda_j)$ $j = 0, \cdots, M-1$, and $\boldsymbol{V}_M$ is the matrix of eigenvectors of the matrix $\boldsymbol{A}_L + \boldsymbol{A}_U$, (with $\lambda_1, \cdots, \lambda_M$ being the corresponding eignevalues).

   It is crucial to remark here that $\boldsymbol{V}_M$ is a constant problem-independent matrix that does not depend on the index p.

2. The second feature of $\tilde{\boldsymbol{K}}_{p,M}$ is that it can be a good approximation to $\boldsymbol{K}_{p,M}$ provided that the polynomials $\psi_{p,M}(\cdot)$ are properly chosen. This feature ensures that replacing $\boldsymbol{K}_{p,M}$ with $\tilde{\boldsymbol{K}}_{p,M}$ will not result in loss of accuracy. We will later provide the form of polynomials, $\psi_{p,M}$ found to be most appropriate for this objective.

The role that the above features play in decoupling $\mathcal{J}_{\text{HB-PC}}$ will be illustrated next. Similar to the approach followed in the previous section, we will first consider this role for the special case of a single random variable ($d = 1$) in Section 4.3, and follow it with the general case of $d > 1$ in Section 4.4.

4.3 Decoupled Structure for Single Random Variable ($d = 1$)

Here, we substitute for $\boldsymbol{K}_{p,M}$ with $\tilde{\boldsymbol{K}}_{p,M}$ in (4.10) and rewrite the alternative Jacobian matrix as follows,

$$\widetilde{\boldsymbol{\mathcal{J}}}_{\text{HB-PC}} = \sum_{p=0}^{M-1} \tilde{\boldsymbol{K}}_{p,M} \otimes \overline{\boldsymbol{\mathcal{J}}}_p + \sum_{p=0}^{M-1} \tilde{\boldsymbol{K}}_{p,M} \otimes \overline{\boldsymbol{\mathcal{Y}}}_p \tag{4.26}$$

Substituting from (5.45) and repeatedly applying the property of the Kronecker product (4.15) transforms (4.26) into

$$\widetilde{\boldsymbol{\mathcal{J}}}_{\text{HB-PC}} = (\boldsymbol{V}_M \otimes \mathbf{I}_{NH}) \left(\sum_{p=0}^{M-1} \boldsymbol{\Psi}_{p,M}(\boldsymbol{\lambda}) \otimes \overline{\boldsymbol{\mathcal{J}}}_p + \sum_{p=0}^{M-1} \boldsymbol{\Psi}_{p,M}(\boldsymbol{\lambda}) \otimes \overline{\boldsymbol{\mathcal{Y}}}_p \right) \left(\boldsymbol{V}_M^{-1} \otimes \mathbf{I}_{NH} \right) \tag{4.27}$$

which can be expanded as

$$\widetilde{\boldsymbol{\mathcal{J}}}_{\text{HB-PC}} = (\boldsymbol{V}_M \otimes \mathbf{I}_{NG}) \, \boldsymbol{\mathcal{L}} \left(\boldsymbol{V}_M^{-1} \otimes \mathbf{I}_{NG} \right) \tag{4.28}$$

The matrix $\boldsymbol{\mathcal{L}}$ in (4.28) is block diagonal with M diagonal blocks.

The following remarks can be made based on (4.28).

- $\widetilde{\boldsymbol{\mathcal{J}}}_{\text{HB-PC}}$ is related to the matrix $\boldsymbol{Y}$, through the similarity transformation operator $\boldsymbol{V}_M \otimes \mathbf{I}_{NH}$ is problem-independent and is therefore available prior to the computation.

- The diagonal blocks of $\boldsymbol{L}$ are given by

$$\sum_{p=0}^{M-1} \psi_{p,M}(\lambda_i)(\overline{\boldsymbol{\mathcal{J}}}_p + \overline{\boldsymbol{\mathcal{Y}}}_p)$$

  for $i = 0, \cdots, M-1$. Those blocks have size NG and are structurally identical (i.e., have identical patterns for the nonzero entries) to the Harmonic Balance Jacobian matrix $\bar{\boldsymbol{J}}_{\text{HB}}$.

This observation follows from the fact that both of $\overline{\boldsymbol{\mathcal{J}}}_p$ and $\overline{\boldsymbol{\mathcal{Y}}}_p$, have identical structures to the matrices $\bar{\boldsymbol{J}}$ and $\bar{\boldsymbol{Y}}$.

- The block coefficients multipliers, i.e. $\psi_{p,M}(\lambda_i)$ are also problem-independent since they depend only on the eigenvalues of the matrix $\boldsymbol{A}_L + \boldsymbol{A}_U$. Thus, they are computed offline, and used for the analysis of all problems.

Now consider using the alternative matrix $\widetilde{\boldsymbol{\mathcal{J}}}_{\text{HB-PC}}$ instead of $\boldsymbol{\mathcal{J}}_{\text{HB-PC}}$ to update the Newton iterative process. It is easy to see that the update, in this case denoted by $\tilde{\boldsymbol{\Delta}}_{\boldsymbol{\mathcal{X}}}^{(i-1)}$, is obtained from

$$\tilde{\boldsymbol{\Delta}}_{\boldsymbol{\mathcal{X}}}^{(i-1)} = \left(\boldsymbol{V}_M \otimes \mathbf{I}_{NG}\right) \boldsymbol{L}^{-1} \left(\boldsymbol{V}_M^{-1} \otimes \mathbf{I}_{NG}\right) \boldsymbol{\mathcal{E}} \left(\overline{\boldsymbol{\mathcal{X}}}^{(i-1)}\right) \tag{4.29}$$

where $\boldsymbol{\mathcal{E}}\left(\overline{\boldsymbol{\mathcal{X}}}\right) = \overline{\boldsymbol{\mathcal{Y}}\boldsymbol{\mathcal{X}}} + \overline{\boldsymbol{\mathcal{F}}}\left(\overline{\boldsymbol{\mathcal{X}}}\right) - \overline{\boldsymbol{\mathcal{B}}}$. Since $\boldsymbol{L}$ is block diagonal, $\boldsymbol{L}^{-1}$ can be computed by simply factorizing the diagonal blocks independently. Moreover, on platforms with multi-core processors, this process can also be executed in parallel, yielding even higher efficiency, by assigning the factorization of each block to a separate thread. Given that each block is independent from other blocks, there is no need for communication between the threads, thereby minimizing this part of overhead (which always reduces the speedup scalability with multi-core, especially for large block sizes (NG)). This feature in the decoupled approach enables significant speedup for the HB-PC approach and extends its applicability to large problems, without losing its basic advantage.

Finally, it is beneficial to stress the key feature that played the pivotal role in achieving the above formulation. This feature is the result of using the matrix $\tilde{\boldsymbol{K}}_{p,M}$ whose eigenvectors are independent of the index p. Indeed, it was this feature that allowed us to factor out a common transformation matrix outside the summations in (4.27).

4.4 Decoupled Structure for Multi-Random Variables ($d > 1$)

Generalizing the decoupling procedure of the previous section to multi-random variables is carried out by first deriving the relation between $\boldsymbol{\mathcal{K}}_{\boldsymbol{\gamma},M}$ and $\boldsymbol{K}_{p,M}$. The following lemma has been developed for this purpose.

Lemma 2. *Assume that Υ_M is defined such that it includes all multi-indices $\boldsymbol{\alpha} \in \mathbb{N}^d$, such that $0 \leq \alpha_i < P_i$ for $i = 1, \cdots, d$. It then follows that*

$$\boldsymbol{\mathcal{K}}_{\boldsymbol{\gamma},M} = \boldsymbol{K}_{\gamma_1,P_1} \otimes \boldsymbol{K}_{\gamma_2,P_2} \otimes \cdots \otimes \boldsymbol{K}_{\gamma_d,P_d} \tag{4.30}$$

It is worth noting here that the matrices $\boldsymbol{K}_{\gamma_i,P_i}$ in (4.30) have size $P_i \times P_i$, thereby making the matrix $\boldsymbol{\mathcal{K}}_{\boldsymbol{\gamma},M}$ have size $M \times M$, where M is given by $\Pi_{i=1}^{d} P_i$.

Similar to the procedure followed earlier to replace $\boldsymbol{\mathcal{J}}_{\text{HB-PC}}$ with the decoupled $\widetilde{\boldsymbol{\mathcal{J}}}_{\text{HB-PC}}$, an alternative matrix, denoted $\widetilde{\boldsymbol{\mathcal{K}}}_{\boldsymbol{\gamma},M}$ and defined by,

$$\widetilde{\boldsymbol{\mathcal{K}}}_{\boldsymbol{\gamma},M} = \tilde{\boldsymbol{K}}_{\gamma_1,P_1} \otimes \tilde{\boldsymbol{K}}_{\gamma_2,P_2} \otimes \cdots \otimes \tilde{\boldsymbol{K}}_{\gamma_d,P_d} \tag{4.31}$$

will be used in (5.33) in place of $\boldsymbol{\mathcal{K}}_{\boldsymbol{\gamma},M}$. Thus, we will have the general decoupled Jacobian as follows

$$\widetilde{\boldsymbol{\mathcal{J}}}_{\text{HB-PC}} = \sum_{\boldsymbol{\gamma} \in \Upsilon_M} \widetilde{\boldsymbol{\mathcal{K}}}_{\boldsymbol{\gamma},M} \otimes \overline{\boldsymbol{\mathcal{J}}}_{\boldsymbol{\gamma}} + \sum_{\boldsymbol{\gamma} \in \Upsilon_M} \widetilde{\boldsymbol{\mathcal{K}}}_{\boldsymbol{\gamma},M} \otimes \overline{\boldsymbol{\mathcal{Y}}}_{\boldsymbol{\gamma}} \tag{4.32}$$

The eigen-decomposition of $\widetilde{\boldsymbol{\mathcal{K}}}_{\boldsymbol{\gamma},M}$ can be written, through using the eigen-decomposition of $\tilde{\boldsymbol{K}}_{p,M}$ and applying property (4.15) of the Kronecker product, as follows

$$\widetilde{\boldsymbol{\mathcal{K}}}_{\boldsymbol{\gamma},M} = \boldsymbol{\mathcal{V}}_M \bar{\boldsymbol{\Psi}}_{\boldsymbol{\gamma},M} \boldsymbol{\mathcal{V}}_M^{-1} \tag{4.33}$$

where

$$\boldsymbol{\mathcal{V}}_M = \boldsymbol{V}_{P_1} \otimes \boldsymbol{V}_{P_2} \otimes \cdots \otimes \boldsymbol{V}_{P_d} \tag{4.34}$$

and $\bar{\boldsymbol{\Psi}}_{\boldsymbol{\gamma},M}$ is a diagonal matrix obtained from

$$\bar{\boldsymbol{\Psi}}_{\boldsymbol{\gamma},M} = \boldsymbol{\Psi}_{\gamma_1,P_1} \otimes \boldsymbol{\Psi}_{\gamma_2,P_2} \otimes \cdots \otimes \boldsymbol{\Psi}_{\gamma_d,P_d}, \tag{4.35}$$

and $\boldsymbol{\Psi}_{\gamma_i,P_i}$ are $P_i \times P_i$ are diagonal matrices.

It is possible to concisely describe the diagonal elements of $\bar{\boldsymbol{\Psi}}_{\boldsymbol{\gamma},M}$ through first denoting the eigenvalues of $\tilde{\boldsymbol{K}}_{\gamma_i,P_i}$ by λ_{j_i}, where $j_i = 0, \ldots, P_i - 1$. With this notation, a diagonal element in $\bar{\boldsymbol{\Psi}}_{\boldsymbol{\gamma},M}$ is given by,

$$\prod_{i=1}^{d} \psi_{\gamma_i,P_i}\left(\lambda_{j_i}\right)$$

Furthermore, such an element will be located at the l^{th} entry on the diagonal,

where

$$l = \sum_{i=1}^{d} j_i \prod_{k=1}^{d-i} P_k$$

It is important here to stress that $\widetilde{\boldsymbol{\mathcal{K}}}_{\boldsymbol{\gamma},M}$ still maintains the same two features of $\tilde{\boldsymbol{K}}_{p,M}$ that enabled the decoupling procedure for the single random variable case. Indeed, the matrix of eigenvectors of $\widetilde{\boldsymbol{\mathcal{K}}}_{\boldsymbol{\gamma},M}$, or $\boldsymbol{\mathcal{V}}_M$, is independent of the entries of the multi-index $\boldsymbol{\gamma}$. This feature allows us to factor out the matrix $\boldsymbol{\mathcal{V}}_M \otimes \mathbf{I}_{NH}$ from the left, and $\boldsymbol{\mathcal{V}}_M^{-1} \otimes \mathbf{I}_{NH}$ from the right, of (4.32), thereby leading to the decoupled Jacobian matrix

$$\widetilde{\boldsymbol{\mathcal{J}}}_{\text{HB-PC}} = \boldsymbol{\mathcal{V}}_M \otimes \mathbf{I}_{NH} \left(\sum_{\boldsymbol{\gamma} \in \Upsilon_M} \bar{\boldsymbol{\Psi}}_{\boldsymbol{\gamma},M} \otimes \left(\overline{\boldsymbol{\mathcal{J}}}_{\boldsymbol{\gamma}} + \overline{\boldsymbol{\mathcal{Y}}}_{\boldsymbol{\gamma}} \right) \right) \boldsymbol{\mathcal{V}}_M^{-1} \otimes \mathbf{I}_{NH} \tag{4.36}$$

which, similar to (4.28), can be represented using the similarity transformation,

$$\widetilde{\boldsymbol{\mathcal{J}}}_{\text{HB-PC}} = \left(\boldsymbol{\mathcal{V}}_M \otimes \mathbf{I}_{NH} \right) \boldsymbol{L} \left(\boldsymbol{\mathcal{V}}_M^{-1} \otimes \mathbf{I}_{NH} \right) \tag{4.37}$$

where $\boldsymbol{L}$ is a block diagonal matrix, whose l^{th} diagonal block is given by

$$\sum_{\boldsymbol{\gamma} \in \Upsilon_M} \prod_{i=1}^{d} \psi_{\gamma_i,P_i}\left(\lambda_{j_i}\right) \left(\overline{\boldsymbol{\mathcal{J}}}_{\boldsymbol{\gamma}} + \overline{\boldsymbol{\mathcal{Y}}}_{\boldsymbol{\gamma}} \right)$$

with the value of the integer l being obtained above.

4.5 Choice of the Polynomials $\psi_{p,M}$

As indicated in Section 4.3 the choice of the polynomials $\psi_{p,M}(\lambda)$ plays an important role in constructing a matrix $\widetilde{\boldsymbol{\mathcal{J}}}_{\text{HB-PC}}$ that captures with good accuracy the original matrix $\boldsymbol{\mathcal{J}}_{\text{HB-PC}}$. It was found that the following polynomials meet that objective.

$$
\begin{aligned}
\psi_{0,M}(\lambda) &= 1, \psi_{1,M}(\lambda) = \lambda \\
\psi_{2,M}(\lambda) &= \lambda^2 - 1, \psi_{3,M}(\lambda) = \lambda^3 - 3\lambda \\
\psi_{4,M}(\lambda) &= \lambda^4 - 6\lambda^2 + 3, \psi_{5,M}(\lambda) = \lambda^5 - 10\lambda^3 + 15\lambda \\
\psi_{6,M}(\lambda) &= \lambda^6 - 15\lambda^4 + 45\lambda^2 - 15
\end{aligned}
$$

The above polynomials were derived, through inspection, by finding the matrix polynomial in $\boldsymbol{A}_L + \boldsymbol{A}_U$ that minimizes the number of non-zero-entries in the difference $\check{\boldsymbol{K}}_i - \boldsymbol{K}_i$ for $i = 1, \cdots, 6$. For values of $i > 6$, a general optimization problem can be formulated to determine the optimum structure of a matrix polynomial in $\boldsymbol{A}_L + \boldsymbol{A}_U$ that minimizes the difference between $\check{\boldsymbol{K}}_i$ and $\boldsymbol{K}_i$. However, it should be stressed that this optimization is done only once where the results are stored and used for all circuits.

The block diagonal matrix $\boldsymbol{L}$ is constructed by substituting the eigenvalues of the matrix $\boldsymbol{A}_L + \boldsymbol{A}_U$ for λ in the above polynomials and using the results as multipliers for the blocks on the diagonal.

4.6 Discussion

This chapter presented a new method in order to statistically characterize the Harmonic Balance (HB) analysis of RF circuits. The proposed approach described in Chapter 4 is based on the concept of generalized Polynomial Chaos (gPC). However, unlike the standard gPC approach, the proposed approach utilizes a novel formulation of the gPC that enables replacing the dense Jacobian matrix of the classic gPC approach with a new block diagonal matrix, whose diagonal blocks have identical structure as that of the original HB Jacobian matrix. The proposed method takes advantage of this feature to reach several orders of magnitude speedup compared to the standard gPC approach. Furthermore, unlike the Monte Carlo analysis, the proposed method does not need thousands of simulation to compute statistical information such as mean value, therefore, it does not suffer from slow convergence.

A new method utilizing a sparse Decoupling technique to extract the statistical information of Intermodulation distortion of RF circuits will be presented in next chapter.

Chapter 5

Statistical Analysis of IMD using Moment Based gPC

In this chapter a new application of decoupled method will be presented allowing to efficiently characterize IMD in RF circuits. First, the general formulation of moment based HB in the presence of random variables will be described, followed by a proposed Moment Based gPC variability Analysis of IM and closed form of Moment-Based-HB Jacobian Matrix. Finally the decoupled method proposed in previous chapter will be applied in order to reduce the computational cost.

5.1 IMD Under Design Parameters Uncertainty

Here, we consider the problem of computing the IMD, where the circuit contains several design parameters whose actual (post fabrication) values are prone to variability due to the uncertainty

surrounding the manufacturing process. To account for this design uncertainty, the HB equations is recast in the following form,

$$\boldsymbol{Y}(\boldsymbol{\xi})\bar{\boldsymbol{X}}(\boldsymbol{\xi}) + \bar{\boldsymbol{F}}(\bar{\boldsymbol{X}}(\boldsymbol{\xi},\alpha),\boldsymbol{\xi}) = \bar{\boldsymbol{B}}_{\text{DC}} + \alpha\bar{\boldsymbol{B}}_{\text{RF}} \tag{5.1}$$

where $\boldsymbol{\xi} \in \mathbb{R}^{\boldsymbol{d}}$ represents a vector of d normalized random parameters, that capture the design uncertainty. As a consequence of the presence of $\boldsymbol{\xi}$, the Taylor series of $\bar{\boldsymbol{X}}$ and $\bar{\boldsymbol{F}}$ are also modified, i.e,

$$\bar{\boldsymbol{X}}(\boldsymbol{\xi},\alpha) = \sum_{n=0}^{q} \boldsymbol{\mathcal{M}}_n(\boldsymbol{\xi})\alpha^n \tag{5.2}$$

$$\bar{\boldsymbol{F}}(\bar{\boldsymbol{X}}(\boldsymbol{\xi},\alpha),\boldsymbol{\xi}) = \sum_{n=0}^{q} \hat{\boldsymbol{F}}_n(\boldsymbol{\mathcal{M}}(\boldsymbol{\xi}),\boldsymbol{\xi})\alpha^n \tag{5.3}$$

to indicate that the system moments and, in turn, IMD are functions of the random parameters that model the uncertainty in the circuit. This fact shows that IMD needs to be regarded as a stochastic process, whose full characterization can be done by computing its Probability Density Function (pdf).

The traditional approach to accomplish this task, is based on the MC, which proceeds by repeatedly computing the moments $\boldsymbol{\mathcal{M}}_n(\boldsymbol{\xi})$, for randomly selected points in the d-dimensional space spanned by the vector $\boldsymbol{\xi}$. Finally, the MC terminates if the computed *statistical* moments (e.g. mean or standard deviation) converge to fixed values.

Although MC has been traditionally used to obtain the statistical information of circuit performance metrics, such as the IIP3, its significant computation cost due to the slow convergence has become the major disadvantage of this method. The main contribution of proposed method is to avoid this difficulty by proposing an alternative approach based on the concepts of generalized Polynomial Chaos (gPC) and moments of the HB response.

5.2 Proposed Moment Based gPC Approach

The proposed approach is based on two main ideas. The first idea is derived from the concept of generalized Polynomial Chaos (gPC) presented in Section 4.4. The other idea is based on the moment-based approach to IMD calculation presented in Section 2.2.2. The presentation of the proposed approach commences with a general overview in the following subsection.

5.2.1 Overview of the Proposed Approach

The core idea in the proposed approach is to express the moments $\boldsymbol{\mathcal{M}}_n(\boldsymbol{\xi})$ in the Askey-Weiner series

$$\boldsymbol{\mathcal{M}}_n(\boldsymbol{\xi}) \approx \sum_{\boldsymbol{\theta} \in \boldsymbol{\Upsilon}_{\boldsymbol{M}}} \boldsymbol{\mathcal{X}}_{n,\boldsymbol{\theta}} \phi_{\theta}(\boldsymbol{\xi}), \tag{5.4}$$

where $\boldsymbol{\mathcal{X}}_{n,\boldsymbol{\theta}} \in \mathbb{R}^{NH}$ are the series coefficients, $\phi(\boldsymbol{\xi})$ is a set of multi-dimensional polynomials that are orthonormal with respect to a probability density function $w(\boldsymbol{\xi})$ with support on χ [12]. Υ_M in defined as a set of multi-indices $\boldsymbol{\theta} \in \mathbb{N}^d$ whose components $(\theta_i, i = 1, \cdots, d)$ satisfy $\theta_i < P_i$. where P is the polynomial order and $M = \prod_{i=1}^{d} P_i$ [30].

The main objective in the proposed approach is to compute the coefficients $\boldsymbol{\mathcal{X}}_{n,\boldsymbol{\theta}}$. Using these coefficients, statistical properties of the IMD are determined. The development of the proposed approach will proceed in the following stages.

- In the first stage, it is shown that computing those coefficients requires mainly factorizing a matrix, denoted $\overline{\boldsymbol{\mathcal{J}}}_{PC}$, with size $NHM \times NHM$.
- The second stage demonstrates that $\overline{\boldsymbol{\mathcal{J}}}_{PC}$ can be written in a closed-form expression using the Kronecker product operator.

- The third and final stage then shows that $\overline{\mathcal{J}}_{PC}$ can be decoupled into matrices whose size is N that can all be factorized independently, resulting in a significant savings in CPU time.

The first stage is presented in the remainder of this section. The other two stages are described in Sections 5.3 and 5.4, respectively.

5.2.2 Computing the Series Expansion Coefficients $\boldsymbol{\mathcal{X}}_{n,\boldsymbol{\theta}}$

Computation of the coefficients $\boldsymbol{\mathcal{X}}_{n,\boldsymbol{\theta}}$ is illustrated for values of n of 0, 1, and $n \geq 2$,

Computing $\boldsymbol{\mathcal{X}}_{0,\boldsymbol{\theta}}$

Substituting from (5.2) and (5.3) into (5.1) setting $\alpha = 0$ yields

$$\boldsymbol{Y}(\boldsymbol{\xi})\boldsymbol{\mathcal{M}}_0(\boldsymbol{\xi}) + \hat{\boldsymbol{F}}_0(\boldsymbol{\mathcal{M}}_0(\boldsymbol{\xi}), \boldsymbol{\xi}) = \bar{\boldsymbol{B}}_{\mathrm{DC}}, \tag{5.5}$$

where $\hat{\boldsymbol{F}}_n(\boldsymbol{\xi})$ collects the moments of the nonlinear part of the HB equations. To compute $\boldsymbol{\mathcal{X}}_{0,\boldsymbol{\theta}}$, $\boldsymbol{\mathcal{M}}_0(\boldsymbol{\xi})$, $\boldsymbol{Y}(\xi)$ and $\hat{\boldsymbol{F}}_{\boldsymbol{0}}(\boldsymbol{\mathcal{M}}_0(\boldsymbol{\xi}), \boldsymbol{\xi})$ are expanded in the Askey-Weiner series similar to (5.4) as follows,

$$\boldsymbol{\mathcal{M}}_0(\boldsymbol{\xi}) \approx \sum_{\boldsymbol{\theta} \in \boldsymbol{\Upsilon}_M} \boldsymbol{\mathcal{X}}_{0,\boldsymbol{\theta}} \phi_{\boldsymbol{\theta}}(\boldsymbol{\xi}), \tag{5.6}$$

$$\boldsymbol{Y}(\boldsymbol{\xi}) \approx \sum_{\boldsymbol{\beta} \in \boldsymbol{\Upsilon}_M} \boldsymbol{\mathcal{Y}}_{\boldsymbol{\beta}} \phi_{\boldsymbol{\beta}}(\boldsymbol{\xi}), \tag{5.7}$$

$$\hat{\boldsymbol{F}}_{\boldsymbol{0}}(\boldsymbol{\mathcal{M}}_0(\boldsymbol{\xi}), \boldsymbol{\xi}) \approx \sum_{\boldsymbol{\beta} \in \boldsymbol{\Upsilon}_M} \boldsymbol{\mathcal{F}}_{0,\boldsymbol{\beta}}(\bar{\boldsymbol{\mathcal{X}}}_0) \phi_{\boldsymbol{\beta}}(\boldsymbol{\xi}). \tag{5.8}$$

Next, (5.6), (5.7) and (5.8) are substituted into (5.5) followed by Galerkin Projection (GP) to eliminate $\boldsymbol{\xi}$ from (5.5). This process results in a larger system of deterministic nonlinear algebraic

equations that can be represented by,

$$\overline{\boldsymbol{\mathcal{Y}}}\,\overline{\boldsymbol{\mathcal{X}}}_0 + \overline{\boldsymbol{\mathcal{F}}}_0(\overline{\boldsymbol{\mathcal{X}}}_0) = \overline{\boldsymbol{\mathcal{B}}}_{\text{DC}}. \tag{5.9}$$

where $\overline{\boldsymbol{\mathcal{X}}}_0$ and $\overline{\boldsymbol{\mathcal{F}}}_0(\overline{\boldsymbol{\mathcal{X}}}_0) \in \mathbb{R}^{NHM}$ are the vectors consisting of the series coefficients $\boldsymbol{\mathcal{X}}_{0,\boldsymbol{\theta}}$ and $\boldsymbol{\mathcal{F}}_{0,\boldsymbol{\beta}}$, respectively. Here, $\overline{\boldsymbol{\mathcal{Y}}} \in \mathbb{R}^{NHM\times NHM}$ is a matrix constructed from the coefficients $\boldsymbol{\mathcal{Y}}_{\boldsymbol{\beta}}$ and $\overline{\boldsymbol{\mathcal{B}}}_{\text{DC}} \in \mathbb{R}^{NHM}$ collects the coefficients of the independent DC sources.

Solving (5.9) for $\overline{\boldsymbol{\mathcal{X}}}_0$ requires forming the Jacobian matrix $\overline{\boldsymbol{\mathcal{J}}}_{PC}$, where

$$\overline{\boldsymbol{\mathcal{J}}}_{PC} = \overline{\boldsymbol{\mathcal{Y}}} + \frac{\partial \overline{\boldsymbol{\mathcal{F}}}_0}{\partial \overline{\boldsymbol{\mathcal{X}}}_0}. \tag{5.10}$$

and iterating using

$$\overline{\boldsymbol{\mathcal{X}}}_0^{(i)} = \overline{\boldsymbol{\mathcal{X}}}_0^{(i-1)} - \bar{\boldsymbol{\mathcal{J}}}_{PC}^{-1}\boldsymbol{\mathcal{E}}\left(\overline{\boldsymbol{\mathcal{X}}}_0^{(i-1)}\right) \tag{5.11}$$

starting from an initial guess $\overline{\boldsymbol{\mathcal{X}}}_0^{(0)}$, where $\boldsymbol{\mathcal{E}}\left(\overline{\boldsymbol{\mathcal{X}}}_0\right) = \overline{\boldsymbol{\mathcal{Y}}}\,\overline{\boldsymbol{\mathcal{X}}}_0 + \overline{\boldsymbol{\mathcal{F}}}_0(\overline{\boldsymbol{\mathcal{X}}}_0) - \overline{\boldsymbol{\mathcal{B}}}_{\text{DC}}$.

Computing $\boldsymbol{\mathcal{X}}_{1,\boldsymbol{\theta}}$

First define $\bar{\boldsymbol{J}}(\boldsymbol{\xi},\alpha)$ as

$$\bar{\boldsymbol{J}}(\boldsymbol{\xi},\alpha) = \frac{\partial \bar{\boldsymbol{F}}(\bar{\boldsymbol{X}}(\boldsymbol{\xi},\alpha),\boldsymbol{\xi}}{\partial \bar{\boldsymbol{X}}(\boldsymbol{\xi},\alpha)} \tag{5.12}$$

and let it be expanded in a Taylor Series in α as shown next,

$$\bar{\boldsymbol{J}}(\boldsymbol{\xi},\alpha) = \sum_{k=0}^{\infty} \boldsymbol{J}_k(\boldsymbol{\xi})\alpha^k \tag{5.13}$$

Computing $\boldsymbol{\mathcal{X}}_{1,\boldsymbol{\theta}}$ is done through substituting from (5.2) and (5.3) into (5.1) and equating the first power of α to obtain,

$$\boldsymbol{Y}(\boldsymbol{\xi})\boldsymbol{\mathcal{M}}_1(\boldsymbol{\xi}) + \hat{\boldsymbol{F}}_1(\boldsymbol{\xi}) = \boldsymbol{B}_{\text{RF}}, \tag{5.14}$$

Given that

$$\hat{\boldsymbol{F}}_1(\boldsymbol{\xi}) = \left.\frac{\partial \bar{\boldsymbol{F}}(\bar{\boldsymbol{X}}(\boldsymbol{\xi},\alpha),\boldsymbol{\xi})}{\partial \boldsymbol{\alpha}}\right|_{\alpha=0} \tag{5.15}$$

$$= \left.\frac{\partial \bar{\boldsymbol{F}}(\bar{\boldsymbol{X}}(\boldsymbol{\xi},\alpha),\boldsymbol{\xi})}{\partial \bar{\boldsymbol{X}}(\boldsymbol{\xi},\alpha)}\frac{\partial \bar{\boldsymbol{X}}(\boldsymbol{\xi},\alpha)}{\partial \alpha}\right|_{\alpha=0} \tag{5.16}$$

$$= \left.\frac{\partial \bar{\boldsymbol{F}}(\bar{\boldsymbol{X}}(\boldsymbol{\xi},\alpha),\boldsymbol{\xi})}{\partial \bar{\boldsymbol{X}}(\boldsymbol{\xi},\alpha)}\boldsymbol{\mathcal{M}}_1(\boldsymbol{\xi})\right|_{\alpha=0} \tag{5.17}$$

it then follows from (5.13) that (5.14) can be rewritten as,

$$\left(\boldsymbol{Y}(\boldsymbol{\xi}) + \bar{\boldsymbol{J}}_0(\boldsymbol{\xi})\right)\boldsymbol{\mathcal{M}}_1(\boldsymbol{\xi}) = \boldsymbol{B}_{\text{RF}}, \tag{5.18}$$

where

$$\bar{\boldsymbol{J}}_0(\boldsymbol{\xi}) = \left.\frac{\partial \bar{\boldsymbol{F}}(\bar{\boldsymbol{X}}(\boldsymbol{\xi},\alpha),\boldsymbol{\xi})}{\partial \bar{\boldsymbol{X}}(\boldsymbol{\xi},\alpha)}\right|_{\alpha=0} \tag{5.19}$$

It can be shown that expanding $\boldsymbol{\mathcal{M}}_1(\boldsymbol{\xi})$ and $\bar{\boldsymbol{J}}_0(\boldsymbol{\xi})$

$$\boldsymbol{\mathcal{M}}_1(\boldsymbol{\xi}) \approx \sum_{\boldsymbol{\theta}\in\boldsymbol{\Upsilon}_M} \boldsymbol{\mathcal{X}}_{1,\boldsymbol{\theta}}\phi_{\boldsymbol{\theta}}(\boldsymbol{\xi}), \tag{5.20}$$

$$\bar{\boldsymbol{J}}_0(\boldsymbol{\xi}) \approx \sum_{\boldsymbol{\beta}\in\boldsymbol{\Upsilon}_M} \boldsymbol{\mathcal{J}}_{0,\boldsymbol{\beta}}\phi_{\boldsymbol{\beta}}(\boldsymbol{\xi}), \tag{5.21}$$

and performing the Galerkin projection on (5.18) results in

$$\bar{\boldsymbol{\mathcal{J}}}_{PC}\overline{\boldsymbol{\mathcal{X}}}_1 = \bar{\boldsymbol{B}}_{\text{RF}}. \tag{5.22}$$

Here, $\overline{\boldsymbol{\mathcal{X}}}_1$ and $\bar{\boldsymbol{B}}_{\text{RF}} \in \mathbb{R}^{NHM}$ are vectors containing Hermite Coefficients of $\boldsymbol{\mathcal{M}}_1(\boldsymbol{\xi})$ and $\boldsymbol{B}_{\text{RF}}$, respectively. One should note here that the matrix $\bar{\boldsymbol{\mathcal{J}}}_{PC}$ arising in this process is the same Jacobian matrix used in computing $\boldsymbol{\mathcal{X}}_{0,\boldsymbol{\theta}}$.

Computing $\boldsymbol{\mathcal{X}}_{n,\boldsymbol{\theta}}, n \geq 2$

Similar to the previous step and following the substitution from (5.2) and (5.3) into (5.1) and equating the n^{th} power of α produces,

$$\boldsymbol{Y}(\boldsymbol{\xi})\boldsymbol{\mathcal{M}}_n(\boldsymbol{\xi}) + \hat{\boldsymbol{F}}_n(\boldsymbol{\xi}) = 0. \tag{5.23}$$

We next show that $\hat{\boldsymbol{F}}_n(\boldsymbol{\xi})$ can be expressed in terms of $\boldsymbol{\mathcal{M}}_p(\boldsymbol{\xi})$ with $p \leq n$ and $\bar{\boldsymbol{J}}_k(\boldsymbol{\xi})$ for $k < n$. To this end, we proceed as follows

$$\frac{\partial \bar{\boldsymbol{F}}(\bar{\boldsymbol{X}}(\boldsymbol{\xi},\alpha),\boldsymbol{\xi})}{\partial \alpha} = \frac{\partial \bar{\boldsymbol{F}}(\bar{\boldsymbol{X}}(\boldsymbol{\xi},\alpha),\boldsymbol{\xi})}{\partial \bar{\boldsymbol{X}}(\boldsymbol{\xi},\alpha)} \frac{\partial \bar{\boldsymbol{X}}(\boldsymbol{\xi},\alpha)}{\partial \alpha} = \bar{\boldsymbol{J}}(\boldsymbol{\xi},\alpha) \frac{\partial \bar{\boldsymbol{X}}(\boldsymbol{\xi},\alpha)}{\partial \alpha}. \tag{5.24}$$

Substitution from (5.3) and (5.13) and continuing,

$$\sum_{k=1}^{q} k\hat{\boldsymbol{F}}_k(\boldsymbol{\xi})\alpha^{k-1} = \sum_{k=0}^{q} \boldsymbol{J}_k(\boldsymbol{\xi})\alpha^k \sum_{k=1}^{q} k\boldsymbol{\mathcal{M}}_k(\boldsymbol{\xi})\alpha^{k-1}, \tag{5.25}$$

Setting $\alpha = 0$ on both sides of (5.25) yields

$$\hat{\boldsymbol{F}}_n(\boldsymbol{\xi}) = \bar{\boldsymbol{J}}_0(\boldsymbol{\xi})\boldsymbol{\mathcal{M}}_n(\boldsymbol{\xi}) + \frac{1}{n}\sum_{k=1}^{n-1}(n-k)\bar{\boldsymbol{J}}_k(\boldsymbol{\xi})\boldsymbol{\mathcal{M}}_{n-k}(\boldsymbol{\xi}), \tag{5.26}$$

By substituting (5.26) into (5.23), one obtains

$$\left(\boldsymbol{Y}(\boldsymbol{\xi}) + \bar{\boldsymbol{J}}_0(\boldsymbol{\xi})\right)\boldsymbol{\mathcal{M}}_n(\boldsymbol{\xi}) = -\frac{1}{n}\sum_{k=1}^{n-1}(n-k)\bar{\boldsymbol{J}}_k(\boldsymbol{\xi})\boldsymbol{\mathcal{M}}_{n-k}(\boldsymbol{\xi}). \tag{5.27}$$

To compute $\boldsymbol{\mathcal{X}}_{n,\boldsymbol{\theta}}, n \geq 2$, the $\boldsymbol{\xi}$-dependent terms are expanded again in the Askey-Weiner series

$$\boldsymbol{\mathcal{M}}_n(\boldsymbol{\xi}) \approx \sum_{\boldsymbol{\theta}\in\boldsymbol{\Upsilon}_M} \boldsymbol{\mathcal{X}}_{n,\boldsymbol{\theta}}\phi_{\boldsymbol{\theta}}(\boldsymbol{\xi}) \tag{5.28}$$

$$\boldsymbol{\mathcal{M}}_{n-k}(\boldsymbol{\xi}) \approx \sum_{\boldsymbol{\theta}\in\boldsymbol{\Upsilon}_M} \boldsymbol{\mathcal{X}}_{n-k,\boldsymbol{\theta}}\phi_{\boldsymbol{\theta}}(\boldsymbol{\xi}) \tag{5.29}$$

$$\bar{\boldsymbol{J}}_k(\boldsymbol{\xi}) \approx \sum_{\boldsymbol{\beta}\in\boldsymbol{\Upsilon}_M} \boldsymbol{\mathcal{J}}_{k,\boldsymbol{\beta}}\phi_{\beta}(\boldsymbol{\xi}), \tag{5.30}$$

Substitution from (5.28)- (5.30) into (5.27) and performing the GP yields

$$\bar{\boldsymbol{\mathcal{J}}}_{PC}\overline{\boldsymbol{\mathcal{X}}}_n = -\frac{1}{n}\left(\sum_{k=1}^{n-1}(n-k)\overline{\boldsymbol{\mathcal{J}}}_k\overline{\boldsymbol{\mathcal{X}}}_{(n-k)}\right). \tag{5.31}$$

where $\overline{\boldsymbol{\mathcal{X}}}_n, \overline{\boldsymbol{\mathcal{X}}}_{n-k} \in \mathbb{R}^{NHM}$ are vectors collecting the coefficients $\boldsymbol{\mathcal{X}}_{n,\boldsymbol{\theta}}$ and $\boldsymbol{\mathcal{X}}_{n-k,\boldsymbol{\theta}}$, respectively.

5.3 Closed-Form Expression for $\overline{\boldsymbol{\mathcal{J}}}_{PC}$

The previous section showed that computing the series expansion of $\boldsymbol{\mathcal{M}}_n(\boldsymbol{\xi})$, i.e. $\boldsymbol{\mathcal{X}}_{n,\boldsymbol{\theta}}$ requires mainly factorizing the matrix $\overline{\boldsymbol{\mathcal{J}}}_{PC}$ followed by Forward/Backward substitutions with right-side vectors that depend on the order n. In this section, we present the closed-form expression for $\overline{\boldsymbol{\mathcal{J}}}_{PC}$. The discussion in this section assumes that specific Askey-Wiener polynomials adopted is the Hermite polynomials, that is

$$\phi_{\boldsymbol{\gamma}}(\boldsymbol{\xi}) = \mathcal{H}_{\boldsymbol{\gamma}}(\boldsymbol{\xi}) = \prod_{i=1}^{d} H_{\gamma_i}(\xi_i) \tag{5.32}$$

where $H_{\gamma_i}$is the γ_i^{th} degree Hermite polynomial. In this case the weighting function is $w(\boldsymbol{\xi}) = e^{-||\boldsymbol{\xi}||^2/2}$, and that the domain of the probability of ξ_i is from $-\infty$ to ∞. However, this assumption is mainly intended to simplify the derivation, and can be extended easily to other systems of polynomials with several modifications.

We first start by considering the $\overline{\boldsymbol{\mathcal{J}}}_{PC}$ that arises from the GP in (5.22) or (5.31). Typically, the GP in either one of those equations is implemented by first substituting from (5.20) and (5.21) into (5.18) and multiplying by $\phi_{\boldsymbol{\gamma}}(\boldsymbol{\xi})w(\boldsymbol{\xi})$, ($\boldsymbol{\gamma}$ being an arbitrary multi-index), integration over probability space χ, then repeating the process for all possible $\boldsymbol{\gamma} \in \boldsymbol{\Upsilon}_{\boldsymbol{M}}$. It has been shown in

[28], that this process results in a matrix that can be expressed as follows,

$$\overline{\boldsymbol{\mathcal{J}}}_{\text{PC}} = \sum_{\boldsymbol{\gamma} \in \boldsymbol{\Upsilon}_M} \left(\boldsymbol{\mathcal{K}}_{\boldsymbol{\gamma},M} \otimes \boldsymbol{\mathcal{Y}}_{\boldsymbol{\gamma}} + \boldsymbol{\mathcal{K}}_{\boldsymbol{\gamma},M} \otimes \boldsymbol{\mathcal{J}}_{0,\boldsymbol{\gamma}} \right). \tag{5.33}$$

The matrices $\boldsymbol{\mathcal{K}}_{\boldsymbol{\gamma},M}$ are $M \times M$ matrices which are described using,

$$\boldsymbol{\mathcal{K}}_{\boldsymbol{\gamma},M} = \left[\Theta_{\boldsymbol{\theta},\boldsymbol{\beta},\boldsymbol{\gamma}} \right]_{\boldsymbol{\theta},\boldsymbol{\beta} \in \boldsymbol{\Upsilon}_M}. \tag{5.34}$$

where

$$\Theta_{\boldsymbol{\theta},\boldsymbol{\beta},\boldsymbol{\gamma}} = \int_{-\infty}^{\infty} \cdots \int_{-\infty}^{\infty} \mathcal{H}_{\boldsymbol{\theta}}(\boldsymbol{\xi}) \mathcal{H}_{\boldsymbol{\beta}}(\boldsymbol{\xi}) \mathcal{H}_{\boldsymbol{\gamma}}(\boldsymbol{\xi}) e^{\frac{-||\boldsymbol{\xi}||^2}{2}} \mathrm{d}\boldsymbol{\xi}. \tag{5.35}$$

It has also been shown in [28], that $\boldsymbol{\mathcal{K}}_{\boldsymbol{\gamma},M}$ can be expressed as,

$$\boldsymbol{\mathcal{K}}_{\boldsymbol{\gamma},M} = \boldsymbol{K}_{\gamma_1,P_1} \otimes \boldsymbol{K}_{\gamma_2,P_2} .. \otimes \boldsymbol{K}_{\gamma_d,P_d}. \tag{5.36}$$

where $\boldsymbol{K}_{\gamma_i,P_i}$ is defined through the following lemma.

Lemma 3. *Let $\boldsymbol{K}_{0,P_i}$ be a $P_i \times P_i$ identity matrix denoted by $\mathbf{I}_{P_i}$. It then follows that $\boldsymbol{K}_{\gamma_i,P_i}$ ($\gamma_i > 0$) is given by,*

$$\boldsymbol{K}_{\gamma_i,P_i} = \boldsymbol{A}_L \boldsymbol{K}_{\gamma_i-1,P_i} + \boldsymbol{K}_{\gamma_i-1,P_i} \boldsymbol{A}_U. \tag{5.37}$$

where

$$\boldsymbol{A}_L = \begin{bmatrix} 0 & \cdots & & 0 \\ 1 & 0 & \cdots & 0 \\ 0 & 1 & 0 & \cdots \\ \vdots & \ddots & \cdots & 0 \\ 0 & \cdots & 1 & 0 \end{bmatrix}, \boldsymbol{A}_U = \begin{bmatrix} 0 & 1 & \cdots & & 0 \\ 0 & 0 & 2 & \cdots & 0 \\ 0 & 0 & 0 & 3 & \cdots \\ \vdots & \ddots & \cdots & 0 & P_i - 1 \\ 0 & \cdots & \cdots & 0 & 0 \end{bmatrix}.$$

A direct conclusion that follows immediately from the above lemma is that $\boldsymbol{K}_{\gamma_i,P_i}$ can be represented, using recursive substitution, as,

$$\boldsymbol{K}_{\gamma_i,P_i} = \sum_{j=0}^{\gamma_i} \frac{\gamma_i!}{(\gamma_i - j)! j!} \boldsymbol{A}_L^j \boldsymbol{A}_U^{\gamma_i - j}. \tag{5.38}$$

We now consider the matrix $\frac{\partial \overline{\boldsymbol{\mathcal{F}}}_0}{\partial \overline{\boldsymbol{\mathcal{X}}}_0}$ used in (5.10) and sexpression similar to the above expressions. To this end, we represent it by the following block-wise notation

$$\frac{\partial \overline{\boldsymbol{\mathcal{F}}}_0}{\partial \overline{\boldsymbol{\mathcal{X}}}_0} = \left[\frac{\partial \boldsymbol{\mathcal{F}}_{0,\boldsymbol{\beta}}}{\partial \boldsymbol{\mathcal{X}}_{0,\boldsymbol{\theta}}}\right]_{\boldsymbol{\beta},\boldsymbol{\theta}\in\boldsymbol{\Upsilon}_M}. \tag{5.39}$$

Using the orthogonality property of the Hermite polynomials on (5.8), $\boldsymbol{\mathcal{F}}_{0,\boldsymbol{\beta}}(\overline{\boldsymbol{\mathcal{X}}}_0)$ can be represented as,

$$\boldsymbol{\mathcal{F}}_{0,\boldsymbol{\beta}}(\overline{\boldsymbol{\mathcal{X}}}_0) = \int_{-\infty}^{\infty}\cdots\int_{-\infty}^{\infty}\hat{\boldsymbol{F}}_{\mathbf{0}}(\boldsymbol{\mathcal{M}}_0(\boldsymbol{\xi}),\boldsymbol{\xi})\mathcal{H}_{\boldsymbol{\beta}}(\boldsymbol{\xi})e^{\frac{-||\boldsymbol{\xi}||^2}{2}}\mathrm{d}\boldsymbol{\xi}. \tag{5.40}$$

Differentiating both sides of (5.40) with respect to $\boldsymbol{\mathcal{X}}_{0,\boldsymbol{\theta}}$ and applying the chain rule yields

$$\frac{\partial \boldsymbol{\mathcal{F}}_{0,\boldsymbol{\beta}}}{\partial \boldsymbol{\mathcal{X}}_{0,\boldsymbol{\theta}}} = \int_{-\infty}^{\infty}\cdots\int_{-\infty}^{\infty}\frac{\partial \hat{\boldsymbol{F}}_{\mathbf{0}}(\boldsymbol{\mathcal{M}}_0(\boldsymbol{\xi}),\boldsymbol{\xi})}{\partial \boldsymbol{\mathcal{M}}_0(\boldsymbol{\xi})}\frac{\partial \boldsymbol{\mathcal{M}}_0(\boldsymbol{\xi})}{\partial \boldsymbol{\mathcal{X}}_{0,\boldsymbol{\theta}}}\mathcal{H}_{\boldsymbol{\beta}}(\boldsymbol{\xi})e^{\frac{-||\boldsymbol{\xi}||^2}{2}}\mathrm{d}\boldsymbol{\xi}$$

Using (5.6) simplifies the above to

$$\frac{\partial \boldsymbol{\mathcal{F}}_{0,\boldsymbol{\beta}}}{\partial \boldsymbol{\mathcal{X}}_{0,\boldsymbol{\theta}}} = \int_{-\infty}^{\infty}\cdots\int_{-\infty}^{\infty}\frac{\partial \hat{\boldsymbol{F}}_{\mathbf{0}}(\boldsymbol{\mathcal{M}}_0(\boldsymbol{\xi}),\boldsymbol{\xi})}{\partial \boldsymbol{\mathcal{M}}_0(\boldsymbol{\xi})}\mathcal{H}_{\boldsymbol{\theta}}(\boldsymbol{\xi})\mathcal{H}_{\boldsymbol{\beta}}(\boldsymbol{\xi})e^{\frac{-||\boldsymbol{\xi}||^2}{2}}\mathrm{d}\boldsymbol{\xi}$$

and further to

$$\frac{\partial \boldsymbol{\mathcal{F}}_{0,\boldsymbol{\beta}}}{\partial \boldsymbol{\mathcal{X}}_{0,\boldsymbol{\theta}}} = \int_{-\infty}^{\infty}\cdots\int_{-\infty}^{\infty}\boldsymbol{J}_0(\boldsymbol{\xi})\mathcal{H}_{\boldsymbol{\theta}}(\boldsymbol{\xi})\mathcal{H}_{\boldsymbol{\beta}}(\boldsymbol{\xi})e^{\frac{-||\boldsymbol{\xi}||^2}{2}}\mathrm{d}\boldsymbol{\xi}.$$

Substituting from (5.21) and using the definition of $\Theta_{\boldsymbol{\theta},\boldsymbol{\beta},\boldsymbol{\gamma}}$

$$\frac{\partial \boldsymbol{\mathcal{F}}_{0,\boldsymbol{\beta}}}{\partial \boldsymbol{\mathcal{X}}_{0,\boldsymbol{\theta}}} \approx \sum_{\boldsymbol{\gamma}\in\boldsymbol{\Upsilon}_M}\Theta_{\boldsymbol{\theta},\boldsymbol{\beta},\boldsymbol{\gamma}}\boldsymbol{\mathcal{J}}_{0,\boldsymbol{\gamma}}. \tag{5.41}$$

Then, by using the definitions of the Kronecker matrix product and by employing (5.41) and (5.34), (5.39) can be expressed as,

$$\frac{\partial \overline{\boldsymbol{\mathcal{F}}}_0}{\partial \overline{\boldsymbol{\mathcal{X}}}_0} \approx \sum_{\boldsymbol{\gamma}\in\boldsymbol{\Upsilon}_M}\boldsymbol{\mathcal{K}}_{\boldsymbol{\gamma},M}\otimes\boldsymbol{\mathcal{J}}_{0,\boldsymbol{\gamma}}. \tag{5.42}$$

5.4 Decoupled Jacobian Matrix

Having described the structure of $\overline{\boldsymbol{\mathcal{J}}}_{PC}$, we now show how this matrix can be decoupled into smaller size matrices which can be factorized independenly and much more efficiently than factorizing the original matrix. The decoupling method is based on replacing $\boldsymbol{\mathcal{K}}_{\boldsymbol{\gamma},M}$ in (5.33) by $\widetilde{\boldsymbol{\mathcal{K}}}_{\boldsymbol{\gamma},M}$, which is given by

$$\tilde{\boldsymbol{\mathcal{K}}}_{\boldsymbol{\gamma},M} = \tilde{\boldsymbol{K}}_{\gamma_1,P_1} \otimes \tilde{\boldsymbol{K}}_{\gamma_2,P_2} .. \otimes \tilde{\boldsymbol{K}}_{\gamma_d,P_d} \tag{5.43}$$

with $\tilde{\boldsymbol{K}}_{\gamma_i,P_i}$ being a $P_i \times P_i$ matrix obtained from a matrix polynomial in $\boldsymbol{A}_L + \boldsymbol{A}_U$. To describe this matrix in more details, we introduce a polynomial $\psi_{\gamma_i}(\lambda), \lambda \in \mathbb{R}$ which is a polynomial of degree γ_i in λ. Thus, $\tilde{\boldsymbol{K}}_{\gamma_i,P_i}$ is given by,

$$\tilde{\boldsymbol{K}}_{\gamma_i,P_i} = \psi_{\gamma_i}\left(\boldsymbol{A}_L + \boldsymbol{A}_U\right). \tag{5.44}$$

Here, $\tilde{\boldsymbol{K}}_{\gamma_i,P_i}$ has two features that are pivotal in decoupling,

1. The first feature is that the matrix of eigenvectors of $\tilde{\boldsymbol{K}}_{\gamma_i,P_i}$ is independent of γ_i. This feature follows from the fact that all the matrices $\tilde{\boldsymbol{K}}_{\gamma_i,P_i}$ are defined as polynomials in $\boldsymbol{A}_L + \boldsymbol{A}_U$ [29]. In other words, $\tilde{\boldsymbol{K}}_{\gamma_i,P_i}$ can be written in the following eigen-decomposition form:

$$\tilde{\boldsymbol{K}}_{\gamma_i,P_i} = \boldsymbol{V}_{P_i} \boldsymbol{\Psi}_{\gamma_i,P_i}(\boldsymbol{\lambda}) \boldsymbol{V}_{P_i}^{-1} \tag{5.45}$$

where $\boldsymbol{\Psi}_{\gamma_i,P_i}(\boldsymbol{\lambda})$ is a diagonal matrix whose diagonal entries are given by $\psi_{\gamma_i}(\lambda_j)$ $j = 0, \cdots, P_i - 1$, and $\boldsymbol{V}_{P_i}$ is the matrix of eigenvectors of the matrix $\boldsymbol{A}_L + \boldsymbol{A}_U$, (with $\lambda_1, \cdots, \lambda_{P_i}$ being the corresponding eignevalues).

It is crucial to remark here that $\boldsymbol{V}_{P_i}$ is a constant matrix that does not depend on the index γ_i, but depends only on the degree P_i used for the i^{th} random variable ξ_i.

2. The second feature of $\tilde{\boldsymbol{K}}_{\gamma_i,P_i}$ is that it can be made to approximate the original $\boldsymbol{K}_{\gamma_i,P_i}$ to a good degree, provided that the polynomials $\psi_{\gamma_i}(\cdot)$ are properly chosen. It was shown in [28] that choosing the following polynmials

$$\begin{aligned}
\psi_0(\lambda) &= 1 \\
\psi_1(\lambda) &= \lambda \\
\psi_2(\lambda) &= \lambda^2 - 1 \\
\psi_3(\lambda) &= \lambda^3 - 3\lambda \\
\psi_4(\lambda) &= \lambda^4 - 6\lambda^2 + 3, \\
\psi_5(\lambda) &= \lambda^5 - 10\lambda^3 + 15\lambda \\
\psi_6(\lambda) &= \lambda^6 - 15\lambda^4 + 45\lambda^2 - 15
\end{aligned}$$

does provide a good accuracy and good matching to $\boldsymbol{K}_{\gamma_i,P_i}$.

As a result of above features, the eigen-decomposition of $\widetilde{\boldsymbol{\mathcal{K}}}_{\boldsymbol{\gamma},\boldsymbol{M}}$ can be written by using the eigen-decomposition of $\tilde{\boldsymbol{K}}_{\gamma_i,P_i}$ and applying property of the Kronecker product, as follows

$$\widetilde{\boldsymbol{\mathcal{K}}}_{\boldsymbol{\gamma},M} = \boldsymbol{\mathcal{V}}_M \bar{\boldsymbol{\Psi}}_{\boldsymbol{\gamma},M} \boldsymbol{\mathcal{V}}_M^{-1}. \tag{5.46}$$

where

$$\boldsymbol{\mathcal{V}}_M = \boldsymbol{V}_{P_1} \otimes \boldsymbol{V}_{P_2} \otimes \cdots \otimes \boldsymbol{V}_{P_d} \tag{5.47}$$

$\bar{\boldsymbol{\Psi}}_{\boldsymbol{\gamma},M}$ is a diagonal matrix obtained from

$$\bar{\boldsymbol{\Psi}}_{\boldsymbol{\gamma},M} = \boldsymbol{\Psi}_{\gamma_1,P_1} \otimes \boldsymbol{\Psi}_{\gamma_2,P_2} \otimes \cdots \otimes \boldsymbol{\Psi}_{\gamma_d,P_d}, \tag{5.48}$$

It is possible to concisely describe the diagonal elements of $\bar{\boldsymbol{\Psi}}_{\boldsymbol{\gamma},M}$ through first denoting the

eigenvalues of $\tilde{\boldsymbol{K}}_{\gamma_i,P_i}$ by λ_{j_i}, where $j_i = 0, \ldots, P_i - 1$. With this notation, a diagonal element in $\bar{\boldsymbol{\Psi}}_{\boldsymbol{\gamma},M}$ is given by $\prod_{i=1}^{d} \psi_{\gamma_i}(\lambda_{j_i})$.

Furthermore, such an element will be located at the l^{th} entry on the diagonal, where $l = \sum_{i=1}^{d} j_i \prod_{k=1}^{d-i} P_k$

It is important here to stress that $\widetilde{\boldsymbol{\mathcal{K}}}_{\boldsymbol{\gamma},M}$ still maintains the same two features of $\tilde{\boldsymbol{K}}_{\gamma_i,P_i}$. Indeed, the matrix of eigenvectors of $\widetilde{\boldsymbol{\mathcal{K}}}_{\boldsymbol{\gamma},M}$, (i.e., $\boldsymbol{\mathcal{V}}_M$), is independent of the entries of the multi-index $\boldsymbol{\gamma}$. This feature enables the proposed alternative matrix (denoted by $\widetilde{\boldsymbol{\mathcal{J}}}_{\text{PC}}$) that is constructed by replacing $\boldsymbol{K}_{\gamma_i,P_i}$ with $\tilde{\boldsymbol{K}}_{\gamma_i,P_i}$ in (5.33), that is

$$\widetilde{\boldsymbol{\mathcal{J}}}_{\text{PC}} = \sum_{\boldsymbol{\gamma} \in \Upsilon_M} \left(\widetilde{\boldsymbol{\mathcal{K}}}_{\boldsymbol{\gamma},M} \otimes \boldsymbol{\mathcal{Y}}_{\boldsymbol{\gamma}} + \widetilde{\boldsymbol{\mathcal{K}}}_{\boldsymbol{\gamma},M} \otimes \boldsymbol{\mathcal{J}}_{\mathbf{0},\boldsymbol{\gamma}} \right). \tag{5.49}$$

to be expressed in the following form,

$$\widetilde{\boldsymbol{\mathcal{J}}}_{\text{PC}} = \boldsymbol{\mathcal{V}}_M \otimes \mathbf{I}_{NH} \left(\sum_{\boldsymbol{\gamma} \in \Upsilon_M} \bar{\boldsymbol{\Psi}}_{\boldsymbol{\gamma},M} \otimes (\boldsymbol{\mathcal{Y}}_{\boldsymbol{\gamma}} + \boldsymbol{\mathcal{J}}_{\mathbf{0},\boldsymbol{\gamma}}) \right) \boldsymbol{\mathcal{V}}_M^{-1} \otimes \mathbf{I}_{NH}. \tag{5.50}$$

which is obtained by factoring out the matrix $\boldsymbol{\mathcal{V}}_M \otimes \mathbf{I}_{NH}$ from the left, and $\boldsymbol{\mathcal{V}}_M^{-1} \otimes \mathbf{I}_{NH}$ from the right, of (5.49), thereby leading to the decoupled matrix which, can be simplified as,

$$\widetilde{\boldsymbol{\mathcal{J}}}_{\text{PC}} = (\boldsymbol{\mathcal{V}}_M \otimes \mathbf{I}_{NH}) \boldsymbol{\mathcal{U}} \left(\boldsymbol{\mathcal{V}}_M^{-1} \otimes \mathbf{I}_{NH} \right) \tag{5.51}$$

where $\boldsymbol{\mathcal{U}}$ is a block diagonal matrix, whose l^{th} diagonal block is given by

$$\sum_{\boldsymbol{\gamma} \in \Upsilon_M} \prod_{i=1}^{d} \psi_{\gamma_i}(\lambda_{j_i}) (\boldsymbol{\mathcal{Y}}_{\boldsymbol{\gamma}} + \boldsymbol{\mathcal{J}}_{\boldsymbol{\gamma}})$$

with the value of the integer l being obtained above.

5.4.1 Summary of the Proposed Approach

The proposed approach can be summarized as follows. First the vector of coefficients $\overline{\boldsymbol{\mathcal{X}}}_n$ are computed by solving (5.9), (5.22) and (5.31) through employing the deocupled Jacobian matrix $\widetilde{\boldsymbol{\mathcal{J}}}_{\text{PC}}$ in place of $\overline{\boldsymbol{\mathcal{J}}}_{\text{PC}}$. To solve a system of equations involving the decoupled matrix $\widetilde{\boldsymbol{\mathcal{J}}}_{\text{PC}}$, only the diagonal blocks of $\boldsymbol{\mathcal{U}}$ need to be factroized independently, and the solution obtained from this factorization is mapped using the transformation matrix $\boldsymbol{\mathcal{V}}_M$. Once $\overline{\boldsymbol{\mathcal{X}}}_n$ are computed, the series expansions of the moments $\boldsymbol{\mathcal{M}}_n$ is constructed using (5.4) and the Volterra Kernels and IMD are computed accordingly as explained in Section 2.2.2.

The explicit conclusion extracted immediately from (5.50) and (5.51) is that $\boldsymbol{\mathcal{U}}$ is a sparse block diagonal due to the fact that each block is constructed from the gPC coefficients of sparse Jacobian matrix $\bar{\boldsymbol{J}}_0$, that can be factorized independently.

Chapter 6

Numerical Examples

In this chapter, numerical examples are provided to validate the proposed decoupling approach. In all of the examples presented in this section, the polynomial coefficients obtained through the proposed approach are used to construct a polynomial-based model in the uncertain circuit design parameters. Subsequently, MC-based evaluations of the polynomial-model using 30,000 values of the design parameters randomly selected in the random design space is carried out to generate the Probability Density Function (pdf) of the circuit output. The pdf obtained in this manner is also compared in each of the examples against the traditional MC simulations of the original circuit and with the same number of simulation points.

In presenting the following simulations, the results obtained from the traditional MC are referred to simply as "Monte-Carlo", while those computed based the gPC are referred to by the type of polynomials (e.g., Hermite) used in the gPC technique for single random problems and gPC basis for multi-random problems. In addition, we adopted a truncation order of 3 for all the examples. Additionally all the MC simulations adopt a 15000 realization except for those

mentioned in the figures.

6.1 Numerical Examples of Decoupled HB-PC

The proposed approach was implemented on a LINUX platform. The computation of the Hermite coefficients of the nonlinear term, i.e. $\boldsymbol{\mathcal{F}}_{\boldsymbol{\beta}}$, $\boldsymbol{\mathcal{J}}_{\boldsymbol{\beta}}$, was implemented using a C++ program. This program was interfaced with a higher level Matlab program that used those coefficients to construct the Jacobian matrices $\boldsymbol{\mathcal{J}}_{\text{HB-PC}}$ and $\widetilde{\boldsymbol{\mathcal{J}}}_{\text{HB-PC}}$ which were used in the standard PC [24] and the proposed decoupled PC techniques, respectively. The results were also compared with a direct Monte Carlo simulation to demonstrate the accuracy of both approaches, the number of MC simulation are chosen to achieve the most possible accuracy in comparison with proposed Decoupled method.

6.1.1 Example 1: Tuned Amplifier Circuit

The tuned amplifier circuit shown in Fig. 6.1 was considered in this example. The MNA formulation for this circuit required $N = 19$ variables. The HB problem was set using a single tone with a fundamental frequency $f_0 = 300$ MHz having 0.1V amplitude, and 10 harmonics in the response ($G = 21$).

The uncertainty in the design of this circuit was introduced through considering the capacitor C_1 to be modelled using two independent random variables, ξ_1, ξ_2, i.e. $C_1 = 10^{-9} \times (1 + \sigma_1\xi_1)\,(33 + \sigma_2\xi_2)$, where ξ_1 and ξ_2 are normalized Gaussian Random variables (i.e. with normal distribution having a zero mean and a unity Variance), and $\sigma_1 = 0.1$ and $\sigma_2 = 0.25$.

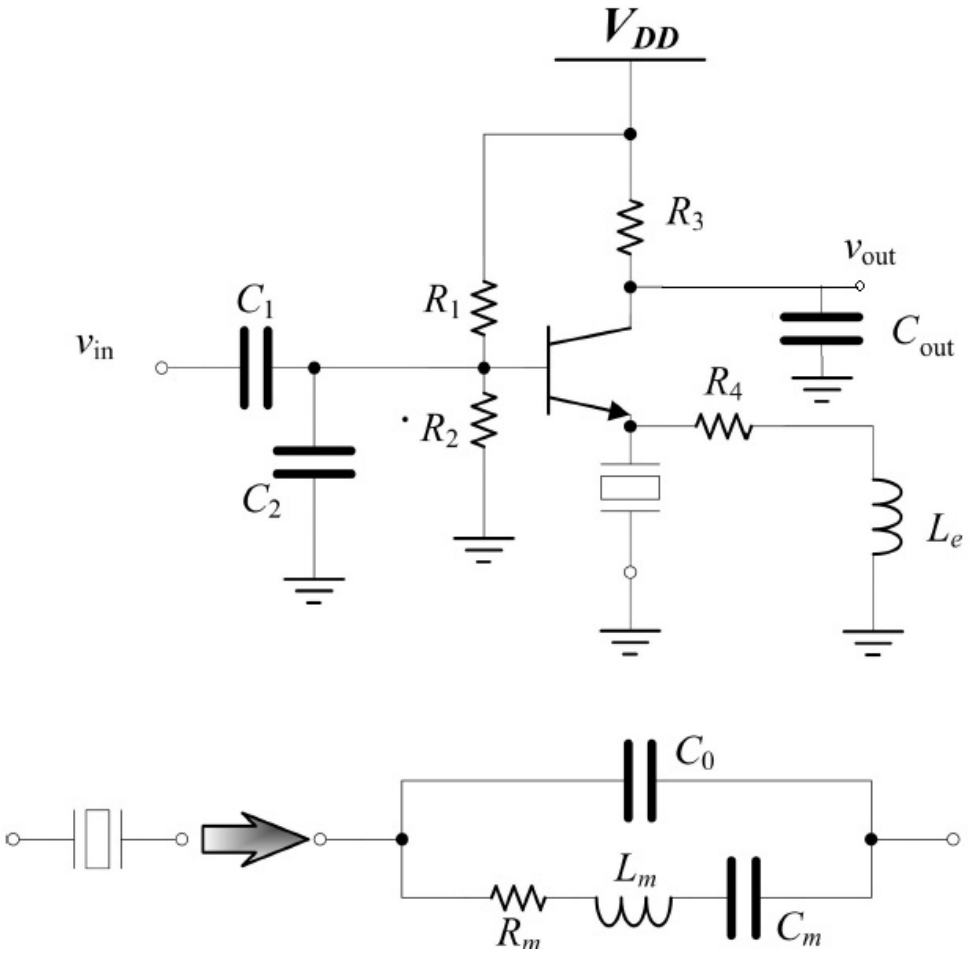

Figure 6.1: Schematic of a tuned amplifier circuit.

Thus, C_1 has a nominal value of 33nF. In addition, the resistance R_1 was also considered to be subject to design uncertainty represented by $R_1 = 4700 \times (1 + \sigma_3 \xi_3)$

Thus, the circuit has $d = 3$ random space. The statistical characterization of its HB response was conducted using the following three distinct approaches.

- The first approach is the *Monte Carlo* approach (MC) which was implemented by solving the HB problem repeatedly until convergence. In this example, MC required 15,000 HB simulations.

- The second approach is the *standard PC* approach. In this approach, a degree 3 Hermite

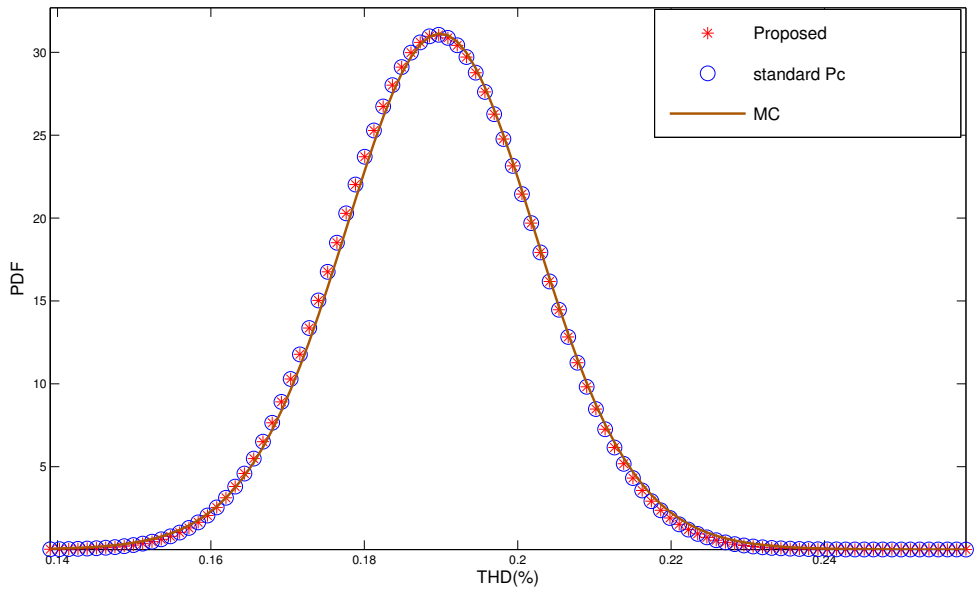

Figure 6.2: Probability density function of the total harmonic distortion (THD) in percentage of the tuned amplifier circuit.

polynomial expansion was used for each random variable making the size of the total Jacobian matrix $\mathcal{J}_{\text{HB-PC}}$ that needs to be factorized to be 25536×25536.

- The third approach is the *proposed decoupling* technique, which required factorizing 64 independent blocks, each with size 399×399.

Table 6.1, first row, shows the mean value computed by the above three approaches for the Total Harmonic Distortion (THD) in %. The first row in Table 6.2 comperes the CPU time taken by the three approaches showing more than two-orders-of-magnitudes speedup obtained by the proposed approach.

To show the overall accuracy of the proposed algorithm achieved at this level of speedup, Fig. 6.2 presents the Probability Density Function (pdf) obtained by the three approaches indicating clearly that the proposed algorithm provides an equivalent level of accuracy as that of the standard

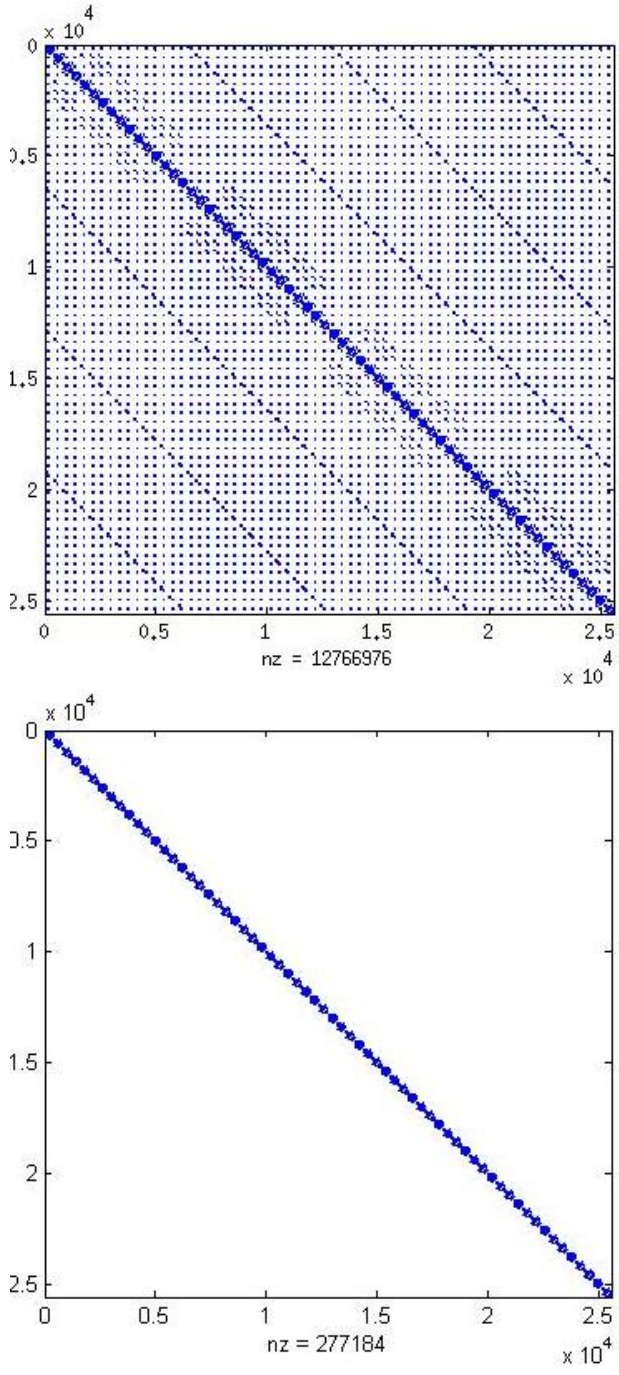

Figure 6.3: Sparsity of $\mathcal{J}_{\text{HB-PC}}$ using the standard PC (Top) and the sparsity pattern of the Jacobian matrix used by the proposed decoupled PC approach $\widetilde{\mathcal{J}}_{\text{HB-PC}}$ (bottom).

PC approach and the traditional Monte Carlo (MC).

To demonstrate the important benefits of the proposed algorithm, sparsity patterns of the resulting Jacobian matrices are compared in Fig. 6.3; the original Jacobian matrix $\mathcal{J}_{\text{HB-PC}}$, (Top panel of Fig. 6.3), and the Jacobian of the proposed approach, $\widetilde{\mathcal{J}}_{\text{HB-PC}}$, (the bottom panel). In addition to the block-diagonal structure of the Jacobian matrix obtained by the proposed approach, this figure shows clearly the significant reduction in the number of nonzero entries.

6.1.2 Example 2: Low-Noise Amplifier

The Low Noise Amplifier (LNA) circuit, shown in Fig. 6.4, is used in this experiment. The LNA was stimulated with a frequency of 160 MHz and the steady-state response was simulated using the HB technique with $G = 21$. The design uncertainty was introduced through representing the input capacitor C_{in} as a parallel-plate capacitor whose physical parameters (length, l, and width, w) are modelled using, $l = l_0\,(1 + 0.1\xi_1)\,, w = w_0\,(1 + 0.1\xi_2)$, where $l_0 = w_0 = 10^{-3}$ (which makes the nominal value of the capacitance of C_{in} equal to 1nF), and ξ_1 and ξ_2 are normalized Gaussian random variables. Another two sources of uncertainty were introduced in the circuit by assuming that R_1 and C_4 are represented, respectively, by $R_1 = 1000 \times (1 + 0.05\xi_3), C_4 = 10^{-9} \times (1 + 0.05\xi_4)$ with ξ_3 and ξ_4 both being normalized Gaussian random variables. The circuit configuration thereby formed a random space with dimensionality $d = 4$, over which the HB results are statistically characterized. In particular, the voltage gain of the circuit was the target of this process, where its PDF was characterized using the proposed approach. The second rows in Tables 6.1 and 6.2 show, respectively, the accuracy and performance of the three approaches indicating that the standard PC approach could not be run due to lack of memory, and

showing that the proposed approach yields a two-orders-of-magnitude speedup compared to the Monte-Carlo approach. To demonstrate the accuracy of the proposed approach, Fig. 6.5 presents a comparison between the PDF obtained using the proposed decoupled PC and the MC-based approach using 15,000 simulations.

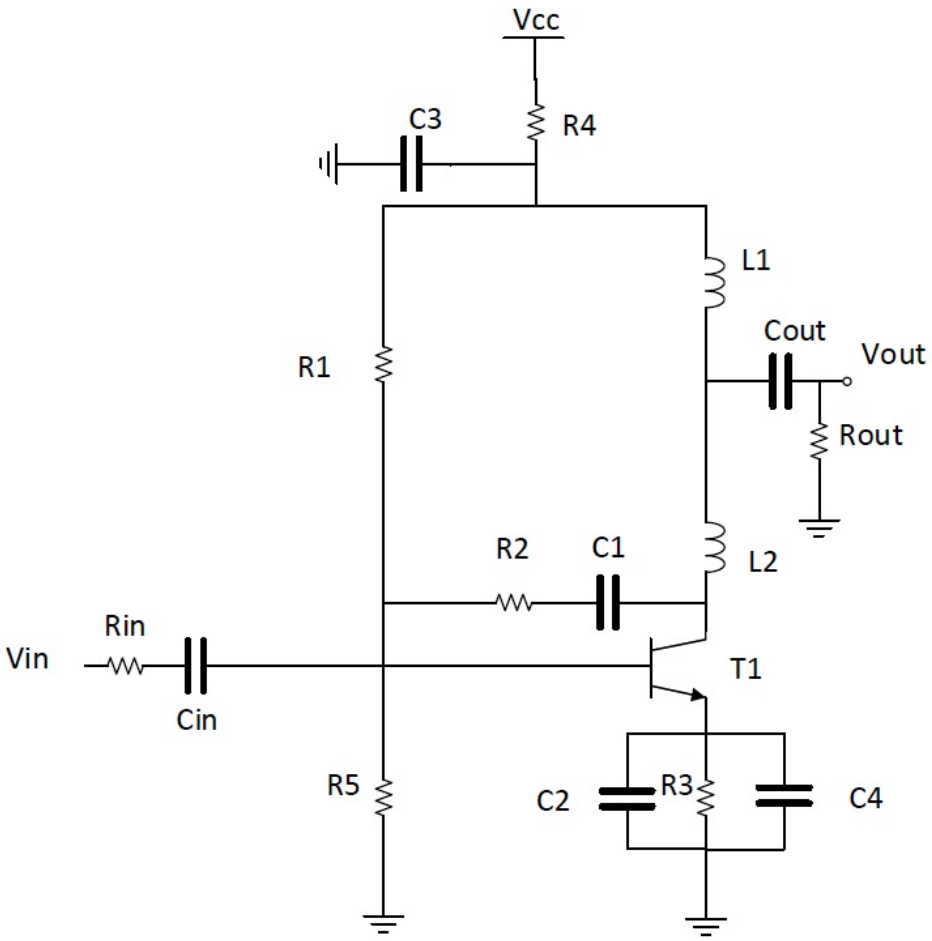

Figure 6.4: Schematic of an LNA circuit

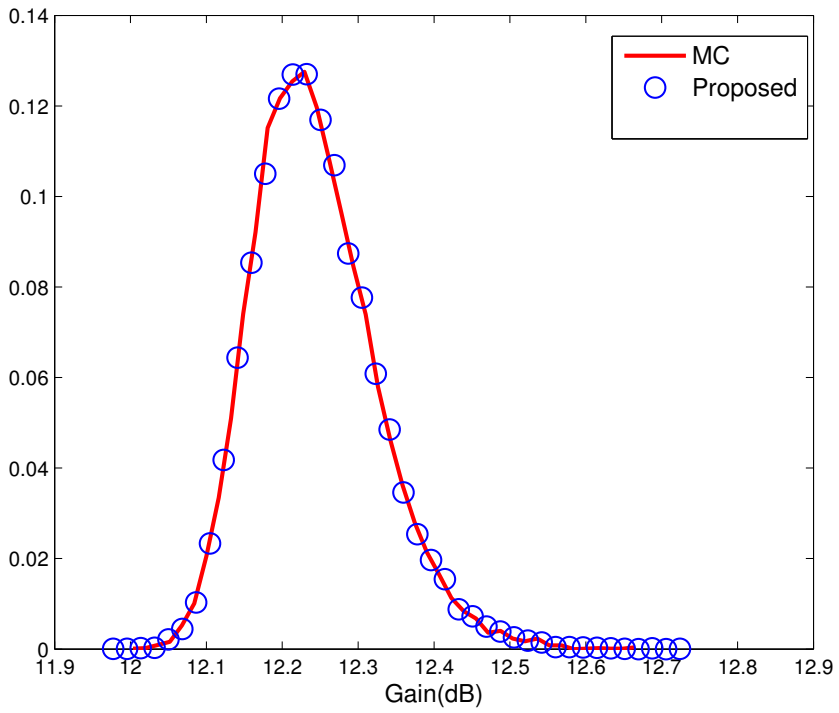

Figure 6.5: Probability distribution function of the Gain (dB) of the LNA circuit.

6.1.3 Example 3: A Mixer Circuit

In this example, a doubly-balanced mixer circuit, shown in Fig. 6.6, was used to validate the proposed algorithm. The MNA size for this circuit is $N = 61$. The circuit was stimulated with three tones ω_{RF1}, ω_{RF2} and ω_{LO} whose values are, respectively, given by, 900MHz, 910MHz, and 1GHz. The spectrum in the response was created using a box truncation scheme with a total of 125 mixing products of the three tones.

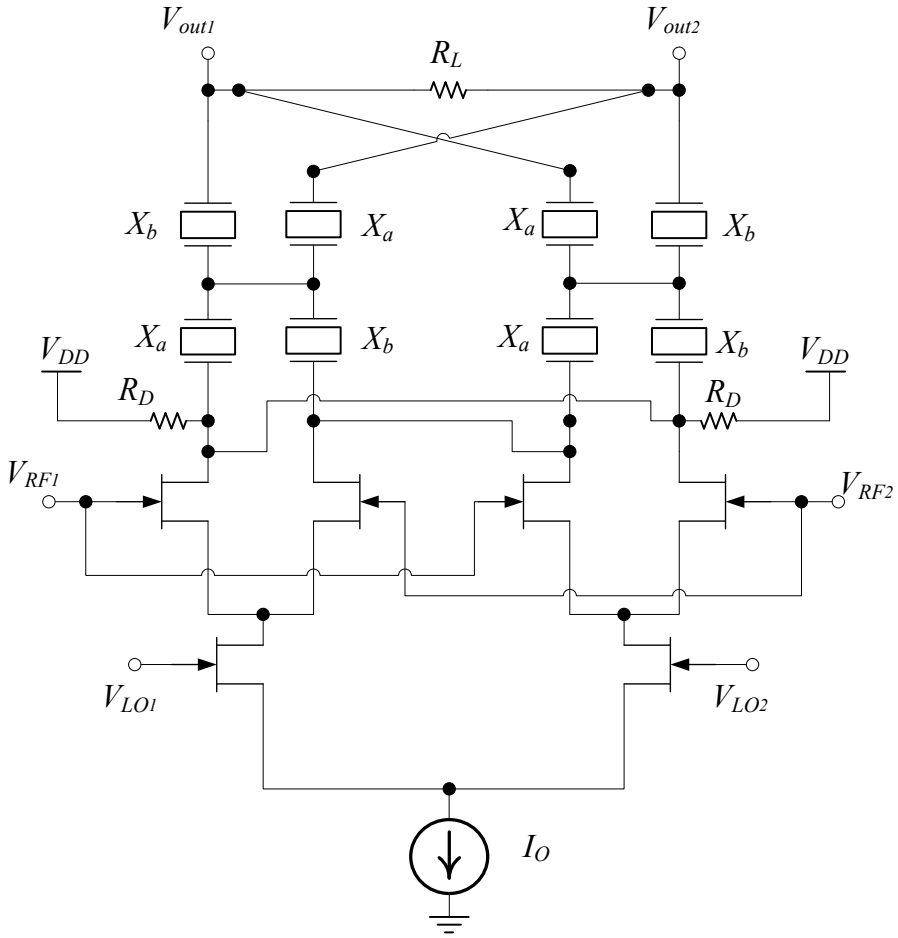

Figure 6.6: A doubly-balanced mixer schematic.

Three sources of uncertainty were introduced in the circuit design, thereby creating a random

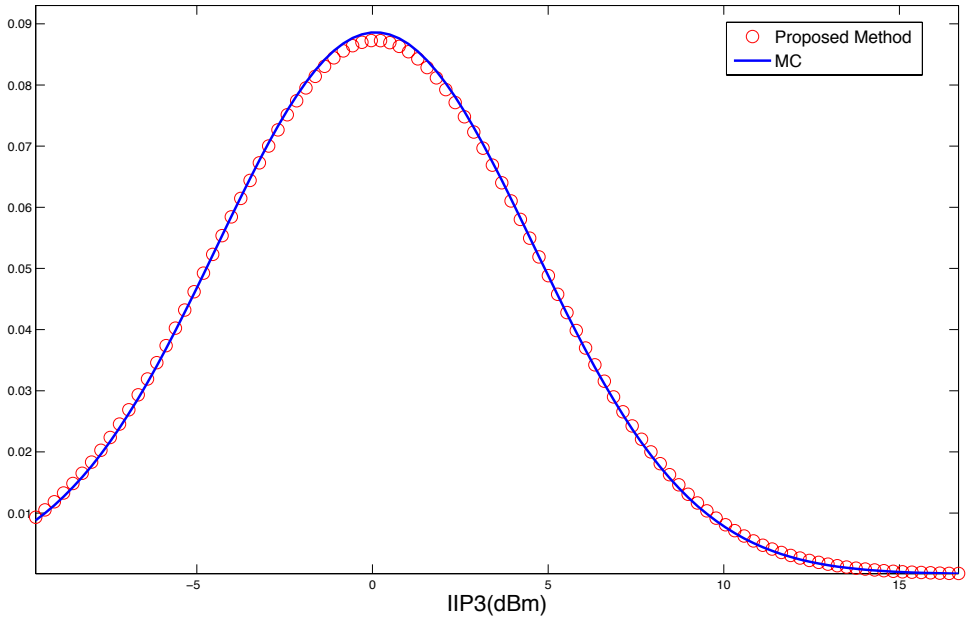

Figure 6.7: Probability Distribution Function of the IIP3 in the mixer circuit.

space with $d = 3$, over which the results of the HB analysis are statistically characterized. Those sources of uncertainty are, the resistances R_D, and R_L, and the capacitance C_{gs} in the JFET model. Those three design parameters were assigned nominal values of $1\text{k}\Omega$, $1\text{k}\Omega$, and 0.27pF, and a standard deviation of $\pm 5\%, \pm 10\%$ and $\pm 10\%$, respectively. The PC problem was then defined by setting $P_i = 3, i = 1, 2, 3$.

The statistical distribution of the third-order intermodulation intercept point (IIP3) was set as the objective in this example. The proposed approach yielded a mean value of -1.74 dBm for IIP3 in 1014 seconds. On the other hand, the standard PC approach could not be carried out due to the excessive memory requirements, while the Monte Carlo approach took several hours of CPU time to reach the similar level of accuracy($< 1\%$ relative error for the mean value).

To demonstrate the accuracy of the proposed approach, Fig. 6.7 presents the pdf of IIP3 obtained from the proposed algorithm and the classical MC approach (with 15,000 simulations).

As seen, the results from both approaches match accurately.

6.2 CPU Time Comparison

This section provides the theoretical computational cost and CPU time comparison for first and second examples. The CPU time was measured using MATLAB R2013a. In the case of circuit simulation, the most time consuming part during the simulation should be the LU decomposition as the computational cost is proportional to the cubic of the matrix size, which will be dominate if the system is large enough.

Table 6.1: Comparison of the mean values: the proposed decoupled PC vs the standard PC approach and Monte carlo.

Example	Monte Carlo	Standard PC	Proposed
Example 1 (THD %))	0.188	0.187	0.187
Example 2 (Gain (dB))	12.237	-	12.235

Table 6.2: Comparison of the CPU time (s) taken by the three approaches.

Example	Monte Carlo	Standard PC	Proposed Method
Tuned Amplifier	1608	867	2.1
LNA	1581	-	4.23

6.3 Numerical Results of Decoupled Moment Based HB-gPC

In this section the numerical results of efficient Decoupled Moment Based HB-gPC are presented. In order to show the efficiency and accuracy of this approach the results are compared with Monte Carlo simulation of Moment Based HB approach. Our algorithm was implemented on a LINUX platform using a C++ program interfaced with a higher level Matlab program to handle the main steps of the proposed approach. The DC bias points in the all circuits were properly selected to minimize the asymmetry phenomenon in the intermodulation products[31]. All the circuits were simulated with the gPC expansion set to $P_i = 3$, which provides sufficient accuracy for all the circuit examples. Results were compared with a traditional Monte Carlo simulation to demonstrate the accuracy and efficiency of the proposed approach.

6.3.1 Example 1. Tuned Amplifier Circuit

The tuned amplifier circuit shown in Fig. 6.1 was considered in this example. This circuit was excited with two tones at -49dBm with fundamental frequencies are $f_1 = 300$ MHz and $f_2 = 301$ MHz. The spectrum in the response was truncated to a set of total 25 mixing products, i.e, H=25. A random design space with $d = 3$ parameters is introduced in this experiment by modelling R_3, C_1 and C_2 . Thusing normal distributions, having mean values of $R_3 = 750\Omega$, $C_1 = 33$nf and $C_2 = 3.3$pf and relative standard deviations of 5%, 15%, and 15%, respectively. The statistical characterization of IMD in this circuit was conducted using two different approaches.

- The first approach is the *Monte Carlo* (MC) approach which was implemented via the moment-based method repeatedly until convergence.

- The second approach is the *proposed Decoupled* technique, which required factorizing 27 independent blocks, each with size 525×525.

The above two approaches were performed to compute the statistical information for Input 2-nd order intercept points (IIP2) and Input 3-rd order intercept points (IIP3). Table 6.3, presents the mean values of IIP2(dBm) and IIP3(dBm) and the CPU time taken by both approaches indicating more than two-orders-of-magnitudes speed-up obtained by the proposed approach. To show the overall accuracy of the proposed approach achieved at this level of speedup, Fig. 6.8 and Fig. 6.9 present the Probability Density Function (pdf) of IIP2 and IIP3 computed using the above method, showing clearly that the proposed algorithm provides an equivalent level of accuracy as that of the traditional Monte Carlo (MC).

Fig. 6.10 shows the sparsity pattern of the decoupled Jacobian of the proposed approach.

Table 6.3: Comparison of the mean values and CPU time of the first example .

	Monte Carlo	Proposed Method
Mean value IIP2(dBm)	11.931	11.926
Mean value IIP3(dBm)	-5.741	-5.737
CPU time (s)	478	0.87

6.3.2 Example 2: Cascode Low-Noise Amplifier

In this experiment a Cascode circuit with nominal gain of 10.5 dB shown in Fig. 6.11 is used to show the performance of the proposed approach. The goal in this experiment is to statistically characterize the $P_{\text{1-dB}}$ compression point in the presence of $d = 4$ random design parameters.

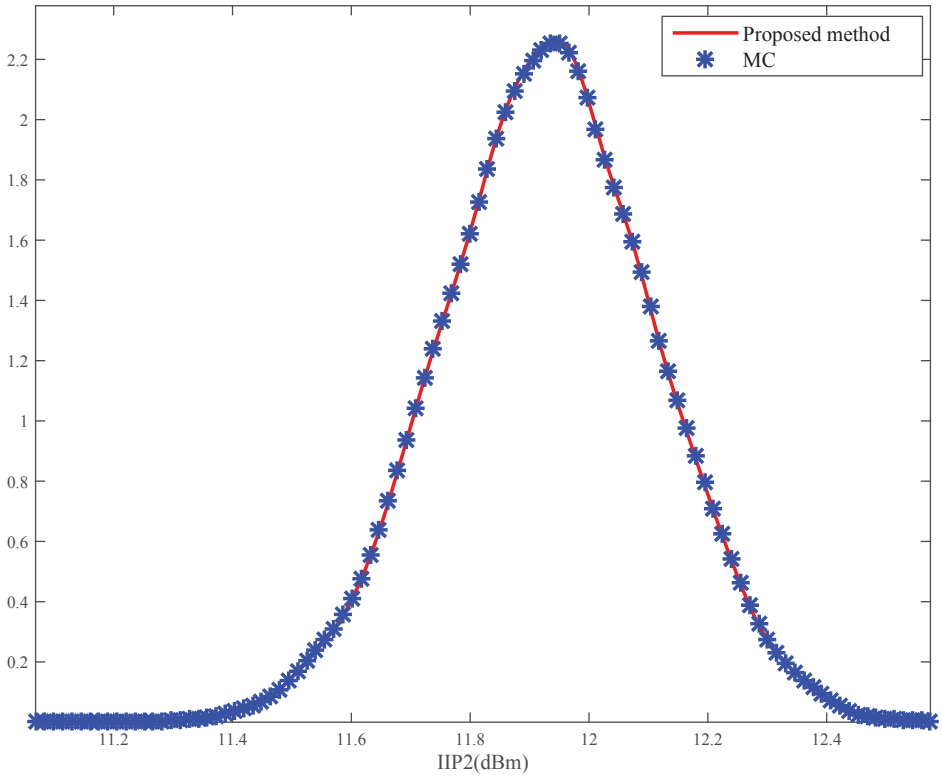

Figure 6.8: Probability density function of the IIP2(dBm) of the tuned amplifier circuit.

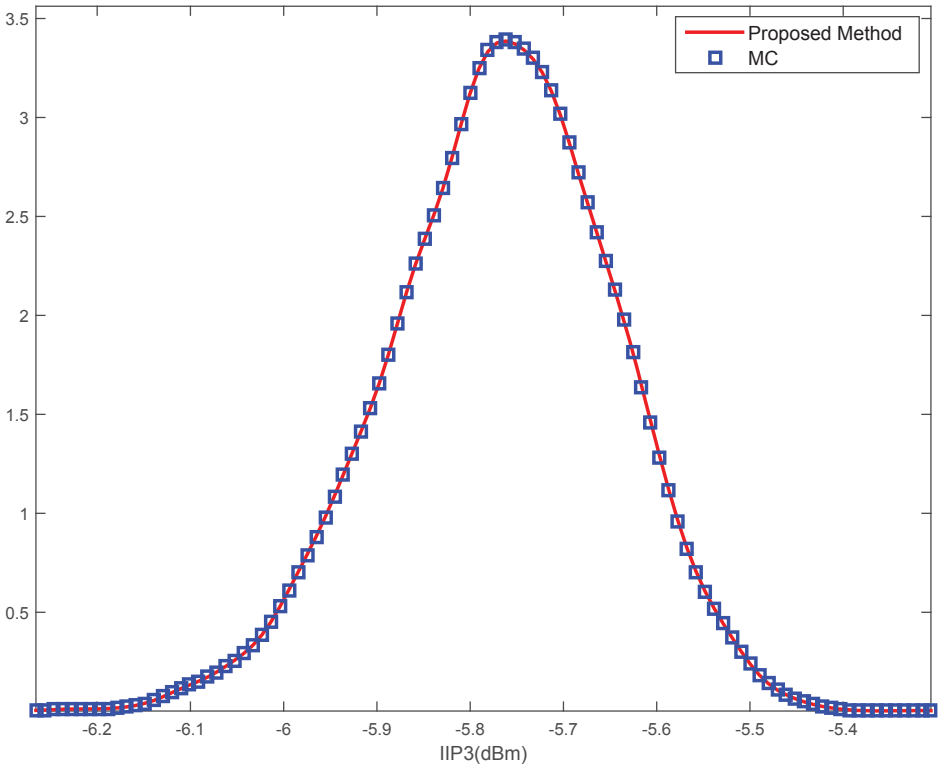

Figure 6.9: Probability density function of the IIP3(dBm) of the tuned amplifier circuit.

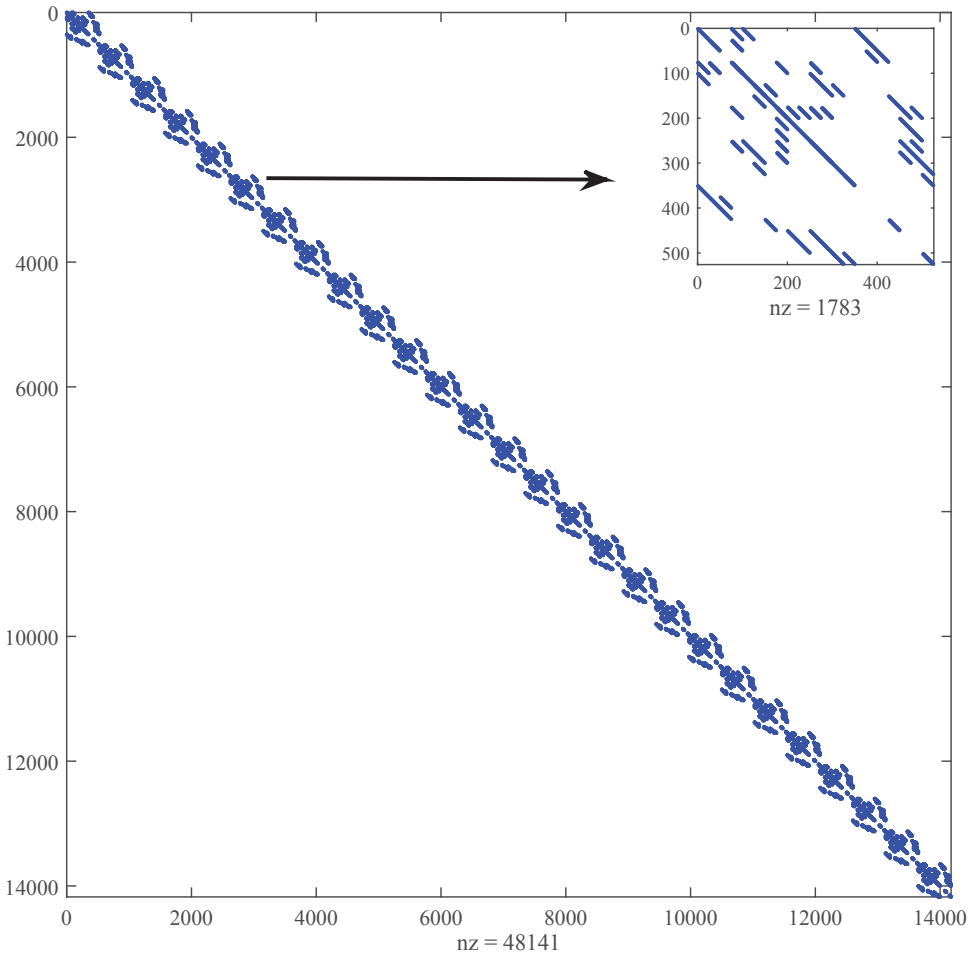

Figure 6.10: Sparsity pattern of the decoupled Jacobian matrix $\widetilde{\mathcal{J}}_{\text{PC}}$ in addition to the the sparsity pattern of 1 block at the top right corner of the figure.

The design parameters considered to be random are L_e, C_c, C_{in} and L_{in}. This parameters were modelled with uniform distribution, having the nominal values $L_e = 1nH$, $C_c = 2.3pf$, $C_{in} = 3.1pf$, $L_{in} = 11nH$ and relative standard deviations 5%, 10%, 10% and 5%, respectively. Two -49dBm tones with the frequencies $f_1 = 800$ MHz and $f_2 = 801$MHz were injected to the circuit whose 25 mixing products construct the spectrum in the response. In this experiment we characterize the pdf of the $P_{\text{1-dB}}(dBm)$ using proposed approach and MC. As clearly can be seen in Fig. 6.12, a good agreement has been exhibited between the two approach. However, MC needed 15000 simulations to reach the same level of accuracy compared with the proposed method whose Jacobian Matrix built from just 81 independent blocks.

Table 6.4 presents the mean values of $P_{\text{1-dB}}(dBm)$ and compares the CPU time between the proposed method and MC where the proposed method shows a significant speed-up over the MC simulation.

Table 6.4: Comparison of the mean values and CPU time of the second example .

	Monte Carlo	Proposed Method
Mean value $P_{\text{1-dB}}(dBm)$	-17.882	-17.871
CPU time (s)	585	3.04

6.3.3 Example 3: Two Stages 10.1dB Low-Noise Amplifier

The third example considered is a two stages low noise amplifier shown in Fig. 6.13 that has been designed to have a nominal voltage gain is 10.1dB. The circuit was stimulated by applying two -49 dBm tones with fundamental frequencies $f_1 = 400$MHz and $f_2 = 401$MHz. The goal

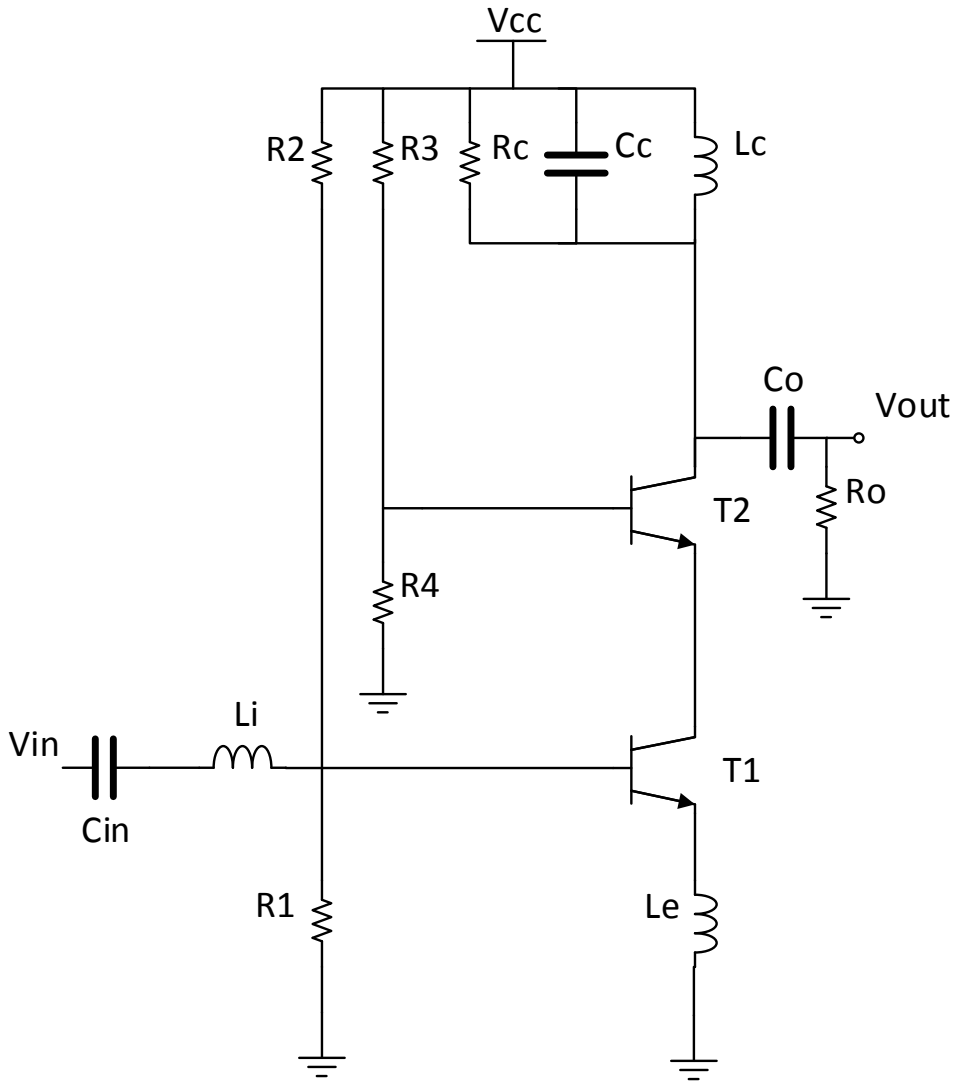

Figure 6.11: Circuit digram in example 2.

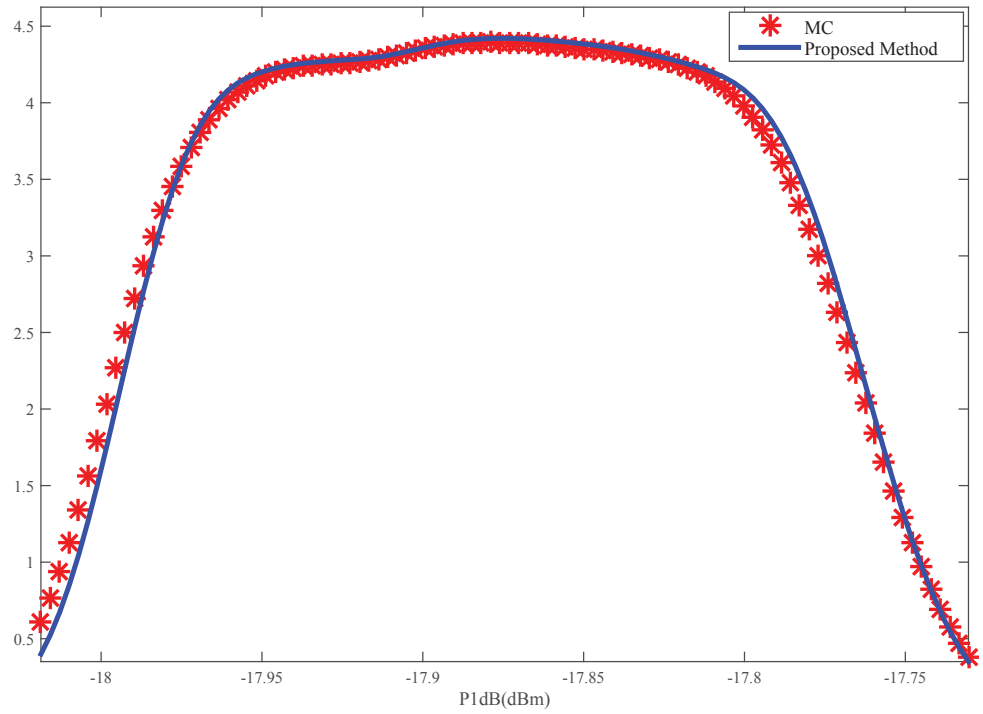

Figure 6.12: Probability density function of the $P_{\text{1-dB}}(dBm)$ of the second example.

of this experiment is to analyze the variability of the output third-order intercept point (OIP3) in the presence of $d = 5$ design uncertainties. The design parameters considered to be random are C_1, C_2, R_6, C_4 and C_3. Here, C_1, C_2, R_6, C_4 were modelled with a normal distributions, having the nominal values of $C_1 = 33nf$, $C_2 = 1nf$, $R_6 = 0.2k\Omega$ and $C_4 = 1pf$ and relative standard deviations of 10%, 10%, 5%, 10%, respectively. On the other hand, C_3 was modelled with uniform distribution, having a nominal value of $1nf$ and relative standard deviations of 15%. The PDF of OIP3 were characterized using the proposed approach and traditional MC approach. As can be clearly seen in Fig. 6.14, both methods show good agreement int the obtained results. Table 6.5, presents the standard deviation and the mean values of OIP3(dBm) and a comparison of CPU time between the Proposed Method and MC, showing a significant speed up achieved by the proposed approach over the traditional MC which required 15,000 simulations to reach the

equivalent level of accuracy.

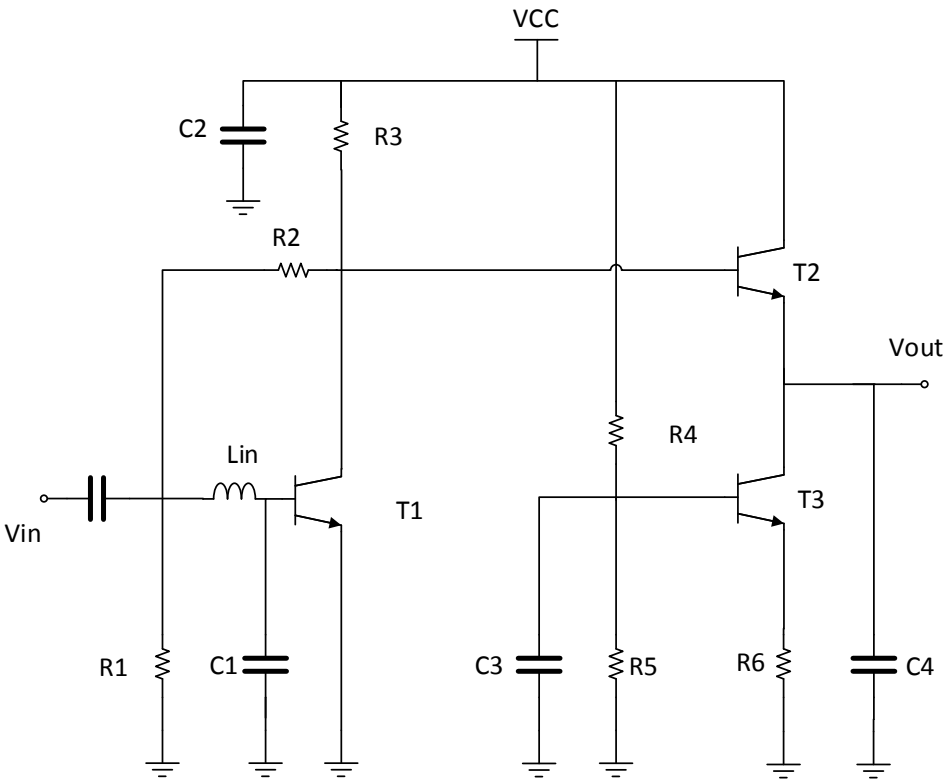

Figure 6.13: Circuit digram in example 2.

Table 6.5: Comparison of the mean values and CPU time of the third example .

	Monte Carlo	Proposed Method
Mean value OIP3(dBm)	5.3511	5.3533
s.t.d value OIP3(dBm)	0.3192	0.3186
CPU time (s)	653	9.31

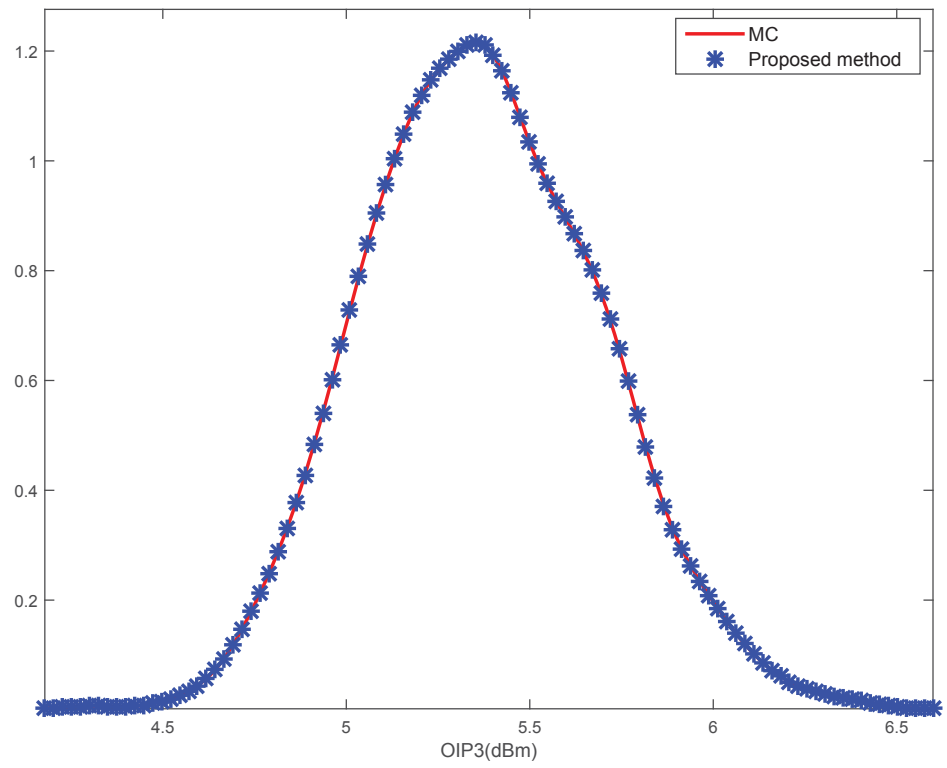

Figure 6.14: Probability density function of the OIP3(dBm) of the third example.

Chapter 7

Conclusion And Future Work

7.1 Conclusion

This thesis first described a new approach for statistical characterization of the Harmonic Balance (HB) analysis. This method is based on the notion of generalized Polynomial Chaos (gPC), however, unlike the standard gPC approach, the proposed decoupled approach utilizes a novel formulation of the gPC that enables replacing the dense Jacobian matrix of the standard gPC approach with a new block diagonal matrix, whose diagonal blocks have identical structure as that of the smaller and original HB Jacobian matrix. This feature in the proposed technique enable several orders of magnitude speedup compared to the standard gPC approach and classic Monte Carlo analysis. Furthermore, a new application of decoupled approach leaded us to obtain a gPC moment based method whose sparse jacobian matrix enabling one to efficiently analyse the statistical information of IMD in RF circuits. The proposed approach therefore retain the advantage of the standard gPC approach over the traditional MC-based approaches, without incurring the

excessive growth in computational cost in the presence of increasing number of uncertainties. Several simulation examples have been presented to demonstrate the gain in speed and efficiency in the proposed approaches without loss of accuracy in the existing approaches.

7.2 Future Work

There are several future work that can be investigated in order to find possible ways to improve the generalized decoupled HB-PC and its extension in characterizing statistical information of IMD in RF circuits.

- Improvement in decoupled gPC: Based on the results presented in this thesis it is quite clear that the decoupled gPC approach has a significant saving in computational cost over the standard gPC approach due to exploiting a block diagonal matrix that each block can be factorized independently. However, there could be a way in order to gain even more efficiency in decoupled gPC. One possible way would be to reduce the number of diagonal blocks that need to be factorized after the decoupling of the augmented matrix. This can be accomplished by either adopting a more efficient truncation scheme or by employing only those blocks whose contribution in the results is more significant.

- Statistical Analysis of IMD in circuits having multi tones excitation such as Mixers: Decoupled moment based gPC to statistically analyze the IMD in RF circuits is presented in this thesis and shown to be more efficient than traditional MC approaches, however, this thesis concentrated on circuits with one tone excitation at their input, such as amplifier circuits. A potential future work would be to seek for a generalized version of decou-

pled moment based gPC approach in order to capture the statistical characterization of RF circuits having several tones excitation as their input, such as mixer circuits.

- Sensitivity analysis: In RF circuit simulation, each circuit component shows a different level of contribution in steady state response and the same situation can be considered in statistical analysis in the presence of design uncertainties. This difference in effectiveness of circuit components and consequently random variables in statistical analysis could lead one to exploit a sensitivity analysis in order to seek for an efficient truncation order in decoupled approach. This approach could save a significant saving in computational cost in decoupled gPC approach.

References

[1] F. Bizzarri, A. Brambilla, and G. S. Gajani, "Steady state computation and noise analysis of analog mixed signal circuits," *IEEE Trans. Circuits and Systems I: Fundamental Theory and Applications*, vol. 59, no. 3, pp. 541–554, 2012.

[2] B. Wang and E. Ngoya, "Integer-N PLLs verification methodology: Large signal steady state and noise analysis," *IEEE Trans. Circuits and Systems I: Fundamental Theory and Applications*, vol. 59, no. 11, pp. 2738–2748, 2012.

[3] L. Iannelli, F. Vasca, and G. Angelone, "Computation of steady-state oscillations in power converters through complementarity," *IEEE Trans. Circuits and Systems I: Fundamental Theory and Applications*, vol. 58, no. 6, pp. 1421–1432, 2011.

[4] J. Liang and W.-H. Liao, "Steady-state simulation and optimization of class-e power amplifiers with extended impedance method," *IEEE Trans. Circuits and Systems I: Fundamental Theory and Applications*, vol. 58, no. 6, pp. 1433–1445, 2011.

[5] A. Brambilla and G. Storti-Gajani, "Frequency warping in time-domain circuit simulation," *IEEE Trans. Circuits and Systems I: Fundamental Theory and Applications*, vol. 50, no. 7, pp. 904–913, 2003.

[6] I. W. Sandberg and G. J. Van Zyl, "Harmonic balance and almost periodic inputs," *IEEE Trans. Circuits and Systems I: Fundamental Theory and Applications*, vol. 49, no. 4, pp. 459–464, 2002.

[7] P. Maffezzoni, "A versatile time-domain approach to simulate oscillators in rf circuits," *Circuits and Systems I: Regular Papers, IEEE Trans*, vol. 56, no. 3, pp. 594–603, 2009.

[8] D. G. Bedrosian and J. Vlach, "An accelerated steady-state method for networks with internally controlled switches," *IEEE Trans. Circuits and Systems I: Fundamental Theory and Applications*, vol. 39, no. 7, pp. 520–530, 1992.

[9] M. Celik, A. Atalar, and M. A. Tan, "A new method for the steady-state analysis of periodically excited nonlinear circuits," *IEEE Trans. Circuits and Systems I: Fundamental Theory and Applications*, vol. 43, no. 12, pp. 964–972, Dec. 1996.

[10] V. Rizzoli, F. Mastri, and D. Masotti, "General noise analysis of nonlinear microwave circuits by the piecewise harmonic-balance technique," *IEEE Trans. Microwave Theory Tech.*, vol. 42, no. 5, pp. 807–819, May 1994.

[11] E. Gad, R. Khazaka, M. S. Nakhla, and R. Griffith, "A circuit reduction technique for finding the steady-state solution of nonlinear circuits," *Microwave Theory and Techniques, IEEE Trans*, vol. 48, no. 12, pp. 2389–2396, 2000.

[12] D. Xiu and G. E. Karniadakis, "The Wiener–Askey polynomial chaos for stochastic differential equations," *SIAM J. Sci. Comput.*, vol. 24, no. 2, pp. 619–644, Feb. 2002.

[13] I. Stievano, P. Manfredi, and F. Canavero, "Carbon nanotube interconnects: Process variation via polynomial chaos," *Electromagnetic Compatibility, IEEE Trans*, vol. 54, no. 1, pp. 140 –148, Feb. 2012.

[14] S. G. Nabavi, E. Gad, M. Nakhla, and R. Achar, "Efficient statistical analysis of microwave circuits using decoupled polynomial chaos," in *Microwave Symposium Digest (MTT), 2014 IEEE MTT-S International*, June 2014.

[15] T.-A. Pham, E. Gad, M. Nakhla, and R. Achar, "Efficient Hermite-based variability analysis using approximate decoupling technique," in *Signal and Power Integrity (SPI), 2013 IEEE 17th Workshop on*, 2013, pp. 111–114.

[16] D. Tannir and R. Khazaka, "Moments-based computation of intermodulation distortion of rf circuits," *Microwave Theory and Techniques, IEEE Trans*, vol. 55, no. 10, pp. 2135–2146, 2007.

[17] S. G. Nabavi, E. Gad, M. Nakhla, and R. Achar, "Statistical analysis of intermodulation distortion in rf circuits using decoupled polynomial chaos," in *International Conference on Numerical Electromagnetic and Multiphysics Modeling and Optimization (NEMO), IEEE MTT-S*, August 2015.

[18] K. Kundert and A. Sangiovanni-Vincentelli, "Simulation of nonlinear circuits in the frequency domain," *IEEE Trans. Computer-Aided Design of Integrated Circ. Sys.*, vol. 5, no. 4, pp. 521–535, Oct. 1986.

[19] K. S. Kundert, J. K. White, and A. Sangiovanni-Vincentelli, *Steady-State Methods for Simulating Analog and Microwave Circuits*. Boston: Kluwer Academic, 1990.

[20] S. A. Maas, *Nonlinear Microwave Circuits*. New York: IEEE Press, 1996.

[21] M. S. Nakhla and J. Vlach, "A piecewise harmonic-balance technique for determination of periodic response of nonlinear systems," *Circuits and Systems I: Fundamental Theory and Applications, IEEE Trans*, vol. 23, no. 2, pp. 85–91, Feb. 1976.

[22] P. Wambacq and W. M. Sansen, *Distortion analysis of analog integrated circuits*. Kluwer Academic Publishers, 1998.

[23] P. Manfredi, "High-speed interconnect models with stochastic parameter variability," Ph.D. dissertation, Politecnico di Torino, 2013.

[24] M. S. Eldred, "Recent advances innon-intrusive polynomial chaos and stochastic collocation methods for uncertainty analysis and design," in *Structures, Structural Dynamics, and Materials Conference*. Sandia National Laboratories, Albuquerque, NM 87185, May 2009.

[25] I. Gradshteyn and I. Ryzhik, *Table of integrals, series and products*. Acadmic Press, 2007, ch. 8, p. 996.

[26] D. Xiu, "Fast numerical methods for stochastic computations: a review," *Communications in computational physics*, vol. 5, no. 2-4, pp. 242–272, 2009.

[27] D. Bernstein, *Matrix Mathematics. Theory, Facts, and Formulas with Applications to Linear Systems Theory*. Princeton University Press, 2005.

[28] T.-A. Pham, E. Gad, M. Nakhla, and R. Achar, "Decoupled polynomial chaos and its applications to statistical analysis of high-speed interconnects," *Components, Packaging and Manufacturing Technology, IEEE Trans*, vol. 4, no. 10, pp. 1634–1647, Oct 2014.

[29] G. H. Golub and C. F. Van Loan, *Matrix Computations*. Johns Hopkins Press, 1989.

[30] G. E. Andrews and R. Askey, "Classical orthogonal polynomials," in *Polynômes orthogonaux et applications*. Springer, 1985, pp. 36–62.

[31] N. B. Carvalho and J. C. Pedro, "Two-tone imd asymmetry in microwave power amplifiers," in *Microwave Symposium Digest. 2000 IEEE MTT-S International*, vol. 1. IEEE, 2000, pp. 445–448.